Assessing the CAM5 physics suite in the WRF-Chem model: implementation, resolution sensitivity, and a first evaluation for a regional case study

P.-L. Ma[1], P. J. Rasch[1], J. D. Fast[1], R. C. Easter[1], W. I. Gustafson Jr.[1], X. Liu[2], S. J. Ghan[1], and B. Singh[1]

[1]Atmospheric Sciences and Global Change Division, Pacific Northwest National Laboratory, Richland, Washington, USA
[2]Department of Atmospheric Science, University of Wyoming, Laramie, Wyoming, USA

Correspondence to: P.-L. Ma (po-lun.ma@pnnl.gov)

Abstract. A suite of physical parameterizations (deep and shallow convection, turbulent boundary layer, aerosols, cloud microphysics, and cloud fraction) from the global climate model Community Atmosphere Model version 5.1 (CAM5) has been implemented in the regional model Weather Research and Forecasting with chemistry (WRF-Chem). A downscaling modeling framework with consistent physics has also been established in which both global and regional simulations use the same emissions and surface fluxes. The WRF-Chem model with the CAM5 physics suite is run at multiple horizontal resolutions over a domain encompassing the northern Pacific Ocean, northeast Asia, and northwest North America for April 2008 when the ARCTAS, ARCPAC, and ISDAC field campaigns took place. These simulations are evaluated against field campaign measurements, satellite retrievals, and ground-based observations, and are compared with simulations that use a set of common WRF-Chem parameterizations.

This manuscript describes the implementation of the CAM5 physics suite in WRF-Chem, provides an overview of the modeling framework and an initial evaluation of the simulated meteorology, clouds, and aerosols, and quantifies the resolution dependence of the cloud and aerosol parameterizations. We demonstrate that some of the CAM5 biases, such as high estimates of cloud susceptibility to aerosols and the underestimation of aerosol concentrations in the Arctic, can be reduced simply by increasing horizontal resolution. We also show that the CAM5 physics suite performs similarly to a set of parameterizations commonly used in WRF-Chem, but produces higher ice and liquid water condensate amounts and near-surface black carbon concentration. Further evaluations that use other mesoscale model parameterizations and perform other case studies are needed to infer whether one parameterization consistently produces results more consistent with observations.

1 Introduction

Global climate models (GCMs) have been used to simulate and understand the mean state and the associated variability of climate, long-term trends of past climate (e.g., Chou et al., 2013; Deser et al., 2012), large-scale climatic response to various forcings (e.g., Ganguly et al., 2012a, b; Gent and Danabasoglu, 2011; Gettelman et al., 2012; Teng et al., 2012), and future climate under different forcing scenarios (e.g., Kravitz et al., 2011; Meehl et al., 2005, 2012). However, it has been challenging for GCMs to accurately capture climate variability such as extreme weather events at regional and local scales (Kang et al., 2002; Zhang et al., 2013). This model deficiency can be attributed not only to the coarse resolution of global models but also to their treatments of physical processes. For example, increasing spatial resolution has been shown to improve simulated climate (Roeckner et al., 2006), precipitation (Giorgi and Marinucci, 1996; Li et al., 2011), and tracer transport (Rind et al., 2007). Yet, some model biases such as the diurnal cycle and spatial pattern of precipitation appear insensitive to spatial resolution, and are attributed to deficiencies in the formulation of physical processes (Iorio et al., 2004; Marshall et al., 1997).

The typical grid size for current GCMs is still rather coarse and ranges from 0.5 to 4 degrees for the atmosphere (Taylor et al., 2012). For example, the Community Atmosphere Model (CAM) version 5 (CAM5) (Neale et al., 2010), the atmospheric component of the Community Earth System Model (CESM) version 1 (Hurrell et al., 2013), typically uses a grid spacing of 1 to 2 degrees. GCMs are expected to take advantage of growing computational resources and run at much higher resolutions in the future. However, the applicability of climate model treatments of physical, chemical, and dynamical processes in a high-resolution setting has not been fully tested, and the resolution dependence of model physics and model biases is not well understood. Rapid development and evaluation of the next generation of CESM requires the ability to isolate processes as well as routinely test parameterizations across a range of scales. Yet, it is computationally expensive to repeatedly conduct long (e.g., multi-year) high-resolution GCM experiments to explore these issues, even on the most powerful modern supercomputers.

The dynamical downscaling approach that uses a relatively high-resolution regional climate model (RCM) has been widely utilized to better represent and understand the climate system at local and regional scales (e.g., Leung and Ghan, 1999a, b; Leung and Qian, 2003; Leung et al., 2003a, b, 2004; Liang et al., 2006). RCMs often focus on reproducing real-world weather events (e.g., Liang et al., 2011; Lin et al., 2011; Ma et al., 2012; Yang et al., 2012), and they are usually run at much smaller grid spacings (e.g., 10 km) over a limited domain for a shorter period of time with high-resolution topography and lateral boundary conditions provided by a GCM or global analyses. Global and regional modeling communities have advanced their modeling techniques independently over the years, with different philosophies and goals. Because RCMs typically operate over smaller timescales and spatial scales, they can explicitly resolve some physical processes that must be parameterized in GCMs. For example, when the Weather Research and Forecasting (WRF) model (Skamarock et al., 2008) is run at mesoscale or cloud-resolving resolutions that can explicitly resolve cloud updrafts, cumulus parameterizations and other subgrid cloud treatments are not required. Detailed spectral bin microphysics schemes can also be employed to better resolve cloud properties and their interactions with aerosols (e.g., Fan et al., 2011), and the vertical transport of tracers can be explicitly resolved as well (e.g., Wang et al., 2004). The WRF model can also be configured as a large eddy simulation model that predicts the super-saturation of air parcels and the activation of cloud condensation nuclei to form cloud droplets based on resolved eddy motions (e.g., Wang and Feingold, 2009a, b), while both RCM and GCM require droplet nucleation parameterization based on parameterized eddy motions (Ghan et al., 1997). At the much coarser resolutions used for global simulations, additional parameterizations are required to account for deep and shallow convections, and the subgrid variability of water substances (Park

et al., 2014; Rasch and Kristjansson, 1998) affecting stratiform clouds. Since parameterizations are generally not as reliable as explicit resolution of processes, one might expect significant improvement for weather, regional climate, and air quality applications when using RCMs at much higher resolution.

Earlier studies have demonstrated that an RCM implemented with GCM parameterizations will show similar behavior and produces similar simulation biases as the host GCM when run at the GCM resolution (Ghan et al., 1999), and that fine-scale features simulated by RCMs at high resolutions are consistent with the same high-resolution GCM results (Laprise et al., 2008). These features make RCMs a good test bed to explore the resolution dependency of fast-physics parameterizations that treat processes with the timescale of hours or less. In addition, high-resolution RCMs simplify direct comparison between observed and simulated quantities (e.g., Haywood et al., 2008). The Aerosol Model Testbed (AMT) (Fast et al., 2011), for example, is one framework that facilitates systematic and objective evaluation of the model simulation of meteorology, clouds, aerosols, and trace gases using various observations including ground-based measurements, aircraft measurements, and satellite retrievals. An RCM configured for a series of test-bed cases might also be used for model calibration of uncertain parameters in the parameterizations, a process that generally requires many simulations, since conducting multiple RCM simulations is relatively inexpensive due to their smaller domain.

However, the dynamical downscaling technique has several issues with respect to the initial and boundary conditions (Wu et al., 2005). For example, the inconsistency of the atmospheric state between a host GCM and an embedded RCM, due to different formulations of physical, chemical, and dynamical processes as well as different resolutions of orography, can produce inconsistent flow patterns at the lateral boundary points of the RCM domain and, ultimately, impact the interior of the domain (Leung, 2012). Even if the GCM and the embedded RCM use the same physics parameterizations, they may not be "resolution-aware" (Gustafson Jr. et al., 2013) and hence can produce different atmospheric states at different resolutions (Skamarock et al., 2012). This problem can be alleviated by using a buffer zone along the lateral boundary (Laprise et al., 2008; Leung et al., 2006; Liang et al., 2001). Model simulations can also be sensitive to perturbations to initial conditions. To address this so-called "internal variability", caused by the internal processes of the model (Caya and Biner, 2004; Giorgi and Bi, 2000), ensemble simulations that increase the signal-to-noise ratio or nudging techniques that constrain large-scale climatology (e.g., Kanamaru and Kanamitsu, 2007; Kooperman et al., 2012; von Storch et al., 2000) can be performed.

The continuous increase of computing power has enabled the scientific community to run GCMs at higher resolutions and to run regional models both at higher resolutions

and over larger domains. Establishing a framework to compare the physics suite implemented in a GCM with other representations implemented in an RCM using systematic and consistent methodology is highly desirable for exploring the strengths and weaknesses of different parameterizations across scales. To take advantage of some of these attributes of RCMs, we have transferred a nearly complete physics suite (including the treatment of deep and shallow convection, cloud microphysics, turbulent boundary layer, aerosols, and fractional clouds) from CAM5 to the WRF model with chemistry (WRF-Chem) (Grell et al., 2005). This modeling framework allows exploration of the parameterization suite at high resolutions with a lower cost than a global model, allows direct comparison of the parameterizations commonly used in cloud/mesoscale models with those used in GCMs, and provides an internally consistent methodology to evaluate various treatments of physics, chemistry, and feedback processes for both types of models. The WRF-Chem model with the CAM5 physics suite can be used in a variety of ways to:

– evaluate the applicability and performance of the CAM5 physics suite in high-resolution settings

– explore the resolution dependence of the CAM5 physics suite

– assess whether biases in the climate model can be reduced solely through increasing model resolution

– perform self-consistent dynamical downscaling simulations by using the same physics in the GCM and RCM so that inconsistencies across the RCM's lateral boundary are greatly reduced

– advance process-level understanding through a systematic comparison between the CAM5 physics and other process representations by utilizing WRF's multiple physics capability

– provide insights into the reformulation of parameterizations towards resolution awareness needed for higher or variable-resolution next-generation GCMs by extracting information of subgrid variability from high-resolution simulations (i.e., make the parameterizations resolution-aware).

In addition to describing how the CAM5 physics suite has been implemented in WRF-Chem, we use this new modeling framework to explore and demonstrate the resolution dependence of simulated cloud properties and aerosol concentrations associated with synoptic conditions that transport anthropogenic and natural aerosols from Asia towards the Arctic. The performance of the CAM5 physics suite is also compared to another set of parameterizations available in the WRF-Chem model to determine whether there are significant differences in simulated clouds and aerosols associated with
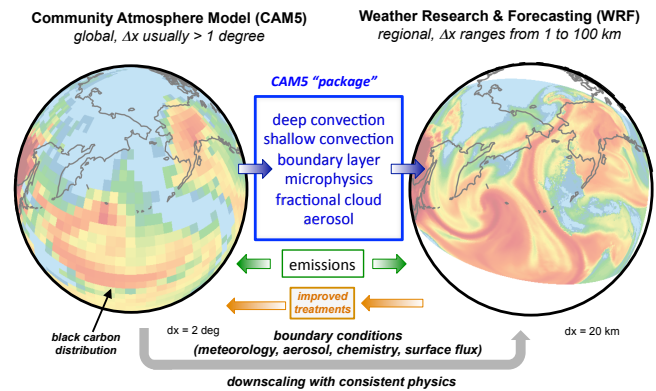

Fig. 1. Schematic diagram of the downscaling modeling framework with consistent physics between CAM5 and WRF.

the parameterizations developed by the global and regional modeling communities.

2 Model implementation

Most of the physics parameterizations from CAM5 (Neale et al., 2010) were transferred to WRF. The suite of parameterizations illustrated in Fig. 1 is introduced through "interface routines" that connect the parent model infrastructure to each parameterization. These interface routines serve the purpose of converting the model state and other variables into the form expected by each parameterization. They determine the shape of arrays to send into the parameterization such as individual columns or 3-dimensional volumes, flip the vertical ordering of arrays, calculate derived variables such as alternate ways of viewing humidity, etc. Both community models employ interface routines, but they are structured differently. Minor modifications to some parameterizations were unavoidable because of differences in the code infrastructure and model design, and occasionally because some fields were already available in WRF so redundant variants were removed (details are provided below). Figure 2 illustrates how the CAM5 physics modules were implemented in WRF. These modules were released in April 2013 as part of WRF (and WRF-Chem) version 3.5, and can be downloaded from the WRF model users website at http://www.mmm.ucar.edu/wrf/users/. The configuration of WRF-Chem running with the CAM5 physics suite has passed a regression test that the model produces the exact same results when using different number of processors.

The specific CAM5 parameterizations ported to WRF include (1) the diagnosed turbulent kinetic energy based first-order K-diffusion moist boundary layer scheme (Bretherton and Park, 2009), (2) the convective inhibition closure based shallow convection scheme (Park and Bretherton, 2009), (3) the consumption of convective available potential energy (CAPE) based Zhang–McFarlane deep convection scheme
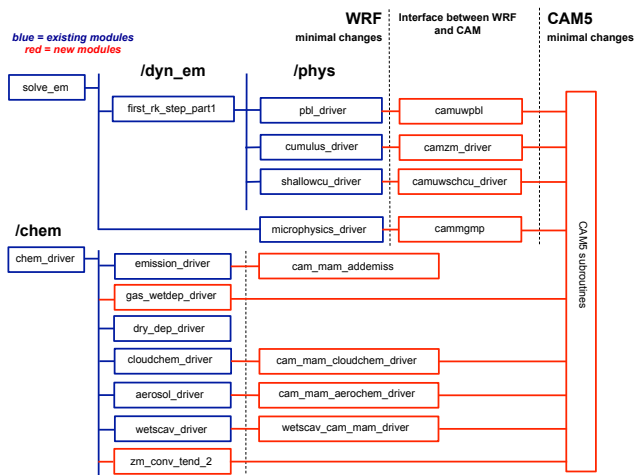
Fig. 2. Partial flow chart of the code implementation of the CAM5 physics suite within the WRF model, where blue denotes existing WRF modules and red denotes modules associated with CAM5 physics and their interfaces with WRF.

(Zhang and Mcfarlane, 1995) with modifications to use a dilute plume to calculate convection depth and CAPE (Neale et al., 2008) and convective momentum transport (Richter and Rasch, 2008), (4) the two-moment cloud microphysics scheme (Gettelman et al., 2008; Morrison and Gettelman, 2008), and (5) the three-mode (Aitken, accumulation, and coarse) version of the Modal Aerosol Module (MAM3) (Liu et al., 2012) that simulates black carbon, mineral dust, sea salt, sulfate, secondary organic aerosols, and primary organic matter. The aerosol direct and indirect effects from CAM5 are also replicated in WRF-Chem. MAM3 in WRF-Chem is coupled with a modified version of carbon-bond mechanism (CBM) gas-phase chemical mechanism called "CBMZ" (Zaveri and Peters, 1999). In contrast, trace gas chemistry in standard CAM5 is simulated with a simple treatment that treats oxidation of sulfur dioxide and dimethyl sulfide as well as production and loss of hydrogen peroxide using climatological values of ozone, and hydroxyl, hydroperoxyl, and nitrate radicals (Neale et al., 2010) from a previously performed Model for OZone and Related Tracers (MOZART) (Emmons et al., 2010) simulation.

CAM5 includes a cloud macrophysics scheme (Park et al., 2014) that treats fractional cloudiness and condensation/evaporation rates within stratiform clouds. The cloud parameterization in WRF typically does not account for fractional clouds, even when used at coarse resolutions that would benefit from such a treatment. The condensation/evaporation rates in WRF are determined by assuming an instantaneous adjustment to saturation. The CAM5 parameterization uses a rather complex treatment of fields produced by other model components in its treatment of these processes. Because the time discretization and the order of parameterization and atmospheric dynamic updates are quite

different between CAM and WRF, porting the CAM5 macrophysics parameterization to WRF is quite difficult. Hence, we implemented a simplified module for the treatment of cloud macrophysics. For stratiform clouds, we implemented the subgrid-scale cloud fraction, condensation, and evaporation using the same triangular probability density function (PDF) formulation as the CAM5 cloud macrophysics scheme. Tunable parameters were set to standard CAM5 values for a 2-degree grid spacing: threshold relative humidity of 88.75 % for low clouds (reduced to 78.75 % for low clouds over land without snow), 80 % for high clouds, and interpolated thresholds for the mid-level clouds. The parameterization produces condensation and evaporation for subgrid clouds with changing cloud fraction (Park et al., 2014; Rasch and Kristjansson, 1998), even if the cell is sub-saturated. The deep and shallow convective cloud fractions are diagnosed from deep and shallow convective mass fluxes, respectively. The treatment of convective detrainment of liquid and ice cloud condensates (both mass and number) follows CAM5, but the detrainment rates in WRF are applied after the convection scheme is called instead of in a separate macrophysics module. When the CAM5 microphysics scheme is selected, the total cloud fraction (the combination of stratiform as well as deep and shallow convective cloud fraction) is computed and used in the radiative transfer calculation by overwriting the standard WRF cloud fraction values calculated in the radiative transfer interface routine (Hong et al., 1998). This simpler macrophysics parameterization produces clouds that are very similar to CAM5, but the implementation was much easier, and it requires minimal code modifications to switch between allowing a continuous cloud fraction (as in CAM5) and binary cloud fraction (as in the traditional WRF) to explore the consequences of the treatment of subgrid clouds (Gustafson Jr. et al., 2013). Changes in cloud fraction between two time steps also result in activation of interstitial aerosol or resuspension of cloud-borne aerosol, respectively (Abdul-Razzak and Ghan, 2000; Liu et al., 2012; Ovtchinnikov and Ghan, 2005), when running WRF-Chem with the MAM3 option.

CAM5 physics integration uses the time splitting approach (Williamson, 2002) that parameterizations are called sequentially, and the state variables are updated after each parameterization is called. However, WRF updates the model state by calling parameterization simultaneously to return a tendency, and updates the state from the tendency sum (parallel process updates, with the exception of cloud microphysics) within the first stage of its Runge–Kutta time integration scheme. We have evaluated the effect of the difference between the call sequence in CAM5 and WRF for a domain encompassing the Pacific storm track by implementing a new code infrastructure that allows WRF to call parameterizations and apply tendencies sequentially, as in CAM5. The results show that the difference of the simulated meteorology, clouds, and aerosols between the sequential and parallel calculation is very small (< 3 %), because WRF uses

very small time steps (e.g., 1 min or less) compared to CAM5 (30 min).

We have embedded the MAM3 as one option of the WRF-Chem, and aerosol processes and their interactions with radiation and clouds follow CAM5 formulations (Ghan et al., 2012; Liu et al., 2012) with a few minor modifications. A slightly different version of the Rapid Radiative Transfer Model for general circulation models (RRTMG) (Iacono et al., 2008; Mlawer et al., 1997) is used, and the existing aerosol optical property module in WRF-Chem (Barnard et al., 2010; Fast et al., 2006), which follows the same methodology and assumptions as CAM5, is employed. Differences between the CAM5 and WRF-Chem aerosol optics codes are negligible, since the formulation and the mixing assumptions (for refractive indices) of the two models are essentially the same. Our package also supports a "prescribed aerosol" option for the cloud microphysics that can be used for configurations of WRF and for WRF-Chem simulations when aerosol–cloud interactions are disabled. In this configuration, the cloud parameterization uses prescribed aerosol numbers and masses for cloud droplet nucleation, with the aerosol mass derived from the prescribed aerosol number and size distribution of each mode.

Multiple aerosol surface deposition velocity calculations are available in WRF-Chem when running with MAM3, and the CAM5 formulation that includes sedimentation, turbulent settling, and molecular adhesivity at the lowest model layer (Zhang et al., 2001) is one available option. However, CAM5 also calculates sedimentation velocities above the lowest model layer, but this is not treated in WRF-Chem. The omission of this process is expected to have very little effect on the life cycle of fine particles (i.e., aerosols in the Aitken and accumulation modes), but may have some effect on the life cycle of the largest particles (i.e., coarse-mode aerosols). The full effect of including sedimentation of aerosols in an RCM requires further investigation.

The MAM aerosol package distinguishes between interstitial and cloud-borne aerosols. In CAM5, advection of cloud-borne aerosols is neglected (Ghan and Easter, 2006). This may produce some error at higher resolution, so we advect both interstitial and cloud-borne aerosols in WRF-Chem.

The convective relaxation timescale (τ) in the deep convection scheme is usually set to be 3600 s in CAM5. With increasing spatial resolution, the model dynamics can produce CAPE at a rate that cannot be removed by the convection with a large τ, producing fallacious "grid-scale storms" (Williamson, 2013). To address this issue, we have introduced a simple formula in WRF version 3.5 to determine τ as a function of grid spacing with a lower bound of 600 s:

$$\tau = \max \left(\tau_{\min}, \tau_{\max} \cdot \frac{\Delta x}{\Delta x_{\mathrm{ref}}} \right),$$

where $\tau_{\min}$ is 600 s, $\tau_{\max}$ is 3600 s, Δx is the grid spacing, and Δx_{ref} is the reference grid spacing, set to be 275 km corresponding to the 2.5 degree grid-spacing in the tropics.

Nonetheless, in this study, we deliberately keep all tunable parameters, including τ, at the same values as used in CAM5 (e.g., $\tau = 3600$ s) for the purpose of exploring the resolution dependence of the parameterizations.

3 From CAM5 to WRF-Chem: the dynamical downscaling procedure

We have developed a dynamical downscaling procedure for this study that (1) minimizes inconsistencies between the parameterizations in the global model CAM5 and the regional model WRF-Chem, (2) facilitates a comparison of simulations between CAM5 and WRF-Chem with CAM5 physic, and (3) produces simulations that agree closely with observed meteorological events. We run CAM5 at a low climate model resolution of 1.9 by 2.5 degree (nominally, "2-degree") grid spacing with 56 levels in the vertical as an "offline model" (Lamarque et al., 2012; Ma et al., 2013b; Rasch et al., 1997), where the model's winds, temperature, and pressure fields are constrained to agree with time interpolated fields from the ERA-Interim reanalysis (Dee et al., 2011), and there is a "wind-mass adjustment" made to the wind fields to make them consistent with the time evolution of the surface pressure field. The offline methodology has been routinely used for studying the atmospheric tracer transport problems (e.g., Ginoux et al., 2001; Jacob et al., 1997; Lawrence et al., 1999; Liu et al., 2009; Ma et al., 2013a). In the offline CAM5 configuration, water substances and aerosols are allowed to evolve freely according to the CAM5 parameterization suite. The model simulation is archived at 6 h intervals. Meteorological fields (winds, temperature, pressure, and humidity), surface fields (winds, temperature, pressure, latent and sensible heat flux, sea surface temperature, and snow height), and tracers (aerosols, trace gases, water vapor, and liquid and ice cloud condensates) are extracted from the archive and used as the initial and boundary conditions for the WRF-Chem simulations. A MOZART simulation is used to provide the initial and boundary conditions for the additional trace gas species in CBMZ. In these simulations, surface latent and sensible heat fluxes from the CAM5 simulation are used to avoid a resolution dependence of the moisture and heat sources, although they could also be calculated within WRF from its surface layer scheme coupled with a land model such as the Community Land Model of the CESM, which is embedded in WRF version 3.5. For the same reason, the effect of topography due to different resolutions is also removed in this study by replacing the standard WRF-Chem topography with the 2-degree CAM5 topography. The vertical sigma coordinate used in WRF is configured to match the sigma-pressure hybrid coordinate used in CAM5 at the initial time step, which has 45 levels from the surface to 20 hPa.

All model configurations use the aerosol emissions from the Polar Study using Aircraft, Remote Sensing, Surface

Measurements and Models, of Climate, Chemistry, Aerosols, and Transport (POLARCAT) Model Intercomparison Project (POLMIP). This inventory was compiled by Louisa Emmons and is available for download at ftp://acd.ucar.edu/user/emmons/EMISSIONS/arctas_streets_finn/. It contains anthropogenic emissions from David Streets' inventory for Arctic Research of the Composition of the Troposphere from Aircraft and Satellites (ARCTAS) (Jacob et al., 2010), biogenic emissions (Granier et al., 2011), and aerosol emissions from fires (Wiedinmyer et al., 2011). However, it does not include some recently identified aerosol sources such as gas flaring and domestic emissions over the Arctic that might result in underprediction of aerosol concentration in the Arctic (Stohl et al., 2013). The POLMIP emission inventory includes mass emissions of primary aerosols, aerosol precursor gases, and other trace gases that are used by CBMZ. The emission data processing follows Liu et al. (2012). A small fraction (2.5 %) of the sulfur sources are emitted as primary sulfate. Anthropogenic sulfate emissions are partitioned 85 %/15 % between the accumulation and Aitken mode, and volcanic sulfate emissions are partitioned 50 %/50 % in those modes. Secondary organic aerosol emissions are produced using fixed yields from isoprene, terpene, toluene, and higher molecular weight alkanes and alkenes precursors. Black carbon, primary organic matter, sulfate, and sulfur emissions from fires are vertically distributed in accordance with the spatially and temporally varied vertical profiles described in the AEROsol model interCOMparison project (AeroCom) (Dentener et al., 2006; Textor et al., 2006). Aerosol number emissions are calculated from mass emissions using the assumed sizes listed in Liu et al. (2012). Emissions of aerosols and trace gases were first apportioned to the CAM5 grid and then regridded to all WRF-Chem grids, so all emissions have the same spatial detail. The MAM3 sea salt and dust emissions are computed online in CAM5 as a function of surface wind speed, and similar parameterizations exist in WRF-Chem as well. However, for the purpose of this paper, we prescribe sea salt and dust emissions in the WRF-Chem with the 6-hourly instantaneous emissions from the CAM5 simulation to eliminate the effect of resolution dependency of these aerosol sources.

4 The aerosol model test-bed case

There have been numerous field campaigns in different regions of the world that could be used to evaluate the performance of the CAM5 physics modules within the regional WRF model framework. We first focus on the high-latitudes because it is a vulnerable region for climate change (e.g., Screen and Simmonds, 2010; Serreze et al., 2009), and there are still large uncertainties regarding the role of aerosols in the Arctic (north of 66.5° N) with documented deficiencies in aerosol transport into the Arctic simulated by GCMs (Lee et al., 2013; Textor et al., 2006; Wang et al., 2013).

To better understand the factors controlling changes in atmospheric composition and climate over the Arctic, several field campaigns were conducted in the vicinity of Alaska during the Arctic haze season (Law and Stohl, 2007; Quinn et al., 2007) in April 2008 as part of the International Polar Year. Three campaigns were conducted, including ARCTAS (Jacob et al., 2010) supported by National Aeronautics and Space Administration (NASA), the Aerosol, Radiation, and Cloud Processes affecting Arctic Climate (ARCPAC) campaign (Brock et al., 2011) supported by National Oceanic and Atmospheric Administration (NOAA), the Indirect and Semi-Direct Aerosol Campaign (ISDAC) (McFarquhar et al., 2011) supported by Department of Energy (DOE), and European campaigns within the POLARCAT project.

An overview of the meteorological conditions observed during the spring of 2008 is described by Fuelberg et al. (2010) and the observed aerosol properties are documented in de Villiers et al. (2010). The ATR-42 (France), Convair-580 (Canada), DC-8 (NASA), G-1 (DOE), P-3B (NASA), and the WP-3D (NOAA) research aircraft sampled meteorological, trace gases, and aerosol quantities using various instruments. Two remote sensing instruments were also deployed: high spectral resolution lidar (HSRL) on the NASA B-200 aircraft that obtained profiles of aerosol backscatter, extinction, and depolarization, and the differential absorption lidar (DIAL) on the DC-8 aircraft that obtained profiles of ozone and aerosol backscatter. Most of the aircraft for ARCTAS, ARCPAC, and ISDAC flew over and in the vicinity of Alaska, and a few DC-8 and WP-3D transects were made over the North Pole and between Alaska and Greenland, while the ATR-42 sampled air masses over northern Scandinavia. In addition to aircraft sampling, routine surface measurements were collected at Barrow, Alaska (71.32° N, 156.62° W), from NOAA's long-term climate research station and DOE's Atmospheric Radiation and Measurement (ARM) climate research facility.

The data collected from these Arctic field campaigns have been merged into a single data set for the AMT, as described in Fast et al. (2011). The AMT consists of the WRF-Chem model and a suite of tools that can be used to evaluate the performance of atmospheric process modules via comparison with a wide variety of field measurements. The "Analysis Toolkit" software (available to the community) extracts simulated variables from model history files in a manner compatible with the available measurements using "instrument simulators". These instrument simulators are used to evaluate the simulated meteorology, clouds, and aerosols from both CAM5 and WRF-Chem by extracting simulated quantities in space and in time to match observations collected along aircraft flight tracks. We focus on comparing the model predictions with black carbon (BC) measurements from the single-particle soot photometers (SP2) and aerosol composition measurements from the aerosol mass spectrometers (AMSs) that were deployed on the DC-8 and P-3B aircraft (Brock et al., 2011; Cubison et al., 2011; McNaughton et al.,

2011; Spackman et al., 2010). Cloud liquid water content and ice water content measured by Convair-580 (Jackson et al., 2012) are used to evaluate the model simulations of clouds.

In addition to the aircraft measurements, we also use other observational data to evaluate the model simulations. For aerosols, we use the surface BC measurements from a particle soot absorption photometer (PSAP) at Barrow, Alaska, and the aerosol optical thickness (AOT) measurements from Aerosol Robotic NETwork (AERONET) (Holben et al., 1998) at Barrow and Bonanza Creek, Alaska. Measurements at the DOE's ARM North Slope of Alaska (NSA) site at Barrow, Alaska, are used to evaluate the simulated clouds. The Liu and Illingworth (2000) retrieval is used to evaluate the ice water content (IWC), and the Liao and Sassen (1994) data product is used to evaluate the liquid water content (LWC). For the column integrated ice water path (IWP) and liquid water path (LWP), we use the ARM Best Estimate (ARMBE) data products (Xie et al., 2010) while acknowledging the fact that multiple retrievals show 20–30 % (for LWP) and 10–60 % (for IWP) uncertainty (Zhao et al., 2012). The ARMBE data product is also used to evaluate the total column precipitable water. To assess the fidelity of the simulated precipitation, we used the 1-degree Global Precipitation Climatology Project (GPCP) daily precipitation data product.

5 Resolution dependence of long-range transport of aerosols and aerosol–cloud interactions

Aerosol–cloud interactions remain one of the largest uncertainties in climate projections. These interactions occur at subgrid scales in most atmospheric models except for large eddy simulations. Deficiencies in the description of these interactions are believed to lead to high estimates of aerosol indirect forcing (Wang et al., 2012) and the underestimation of aerosol concentrations in remote regions such as the Arctic (Koch et al., 2009; Lee et al., 2013; Rasch et al., 2000; Shindell et al., 2008; Textor et al., 2006; Wang et al., 2013). The aerosol indirect forcing can also be amplified due to data aggregation from grid-box averages (McComiskey and Feingold, 2012). Increasing model resolution to reduce the subgrid inhomogeneity and to better resolve aerosol plumes (Weigum et al., 2012) may reduce this model bias. In this section, we document the resolution dependence of aerosol concentration and aerosol–cloud interactions in a high latitude region.

The offline CAM5 simulation was started on 1 January 2008. Water vapor, condensate, and aerosol fields were allowed to spin up for 3 months, and simulation results from 1 April to 1 May 2008 were analyzed and used for initial and boundary conditions for regional downscaling modeling. The regional modeling domain encompasses northeastern Asia, the northern Pacific Ocean, and northwestern North America (Fig. 1, right panel) so that the primary aerosol transport pathway from Asia to Alaska (Ma et al., 2013a, b)

is included. For all our WRF-Chem simulations, the winds and temperature were nudged towards the offline CAM5 fields (which comes from the ERA-Interim reanalysis) using a timescale of 1 hour to constrain those fields to be close to the large-scale analyzed fields since our focus was the life cycle of aerosols and clouds. Simulations were performed using horizontal grid spacings of 160, 80, 40, 20, and 10 km (labeled as WRF_160 km, WRF_80 km, WRF_40 km, WRF_20 km, and WRF_10 km, respectively) to explore the behavior of the cloud and aerosol parameterizations as a function of grid spacing. Note that since the lowest resolution of WRF-Chem used in this study (160 km) is still finer than the CAM5 grid (1.9 by 2.5 degrees) in the mid-latitudes where most aerosol emissions and wet scavenging take place, there might be differences between these two model simulations. In addition, the differences in dynamical cores and time steps between the two models might also contribute to different results.

Figure 3 shows that the simulated meteorology agrees well with the ARCTAS DC-8 aircraft measurements for both the nudged winds and temperature and then freely evolving water vapor mixing ratio at all altitudes around Alaska. There is a 2-degree temperature difference between model simulations and aircraft measurements at higher altitudes (Fig. 3c) that appears to be due to the disagreement between the average temperature within the model layer (typically about 600 m thick at 500 hPa) regridded from the ERA-Interim reanalysis and the instantaneous temperature measurements. As expected, the winds and temperatures from the WRF-Chem simulations are similar to those from CAM5 with no systematic bias associated with resolution. For clouds, it is challenging to simulate the condensate values exactly when and where they occur along an aircraft flight path given the large spatial and temporal variability of clouds as shown in Fig. 4a and b. Therefore, we have also summarized the performance of simulated in-cloud LWC and IWC along 15 Convair-580 flights in terms of the 95th, 75th, 50th, 25th, and 5th percentiles as a function of the model grid spacing (Fig. 4c and d). The simulated median instantaneous in-cloud LWC and IWC are generally within the range of the aircraft measurements. Model simulations occasionally exhibit large in-cloud IWC values when the ice cloud fraction is small and/or snow takes place. The LWC for the CAM5 and 160 km WRF-Chem simulations is about 1 order of magnitude lower than observations. This bias is reduced with increasing resolution; the model mean values are within a factor of 3 for the 10 km simulation. A possible explanation for the increase of cloud liquid water content with increasing resolution is that the moisture convergence is larger in the high-resolution simulation, resulting in higher production of liquid condensates. Further diagnostics is needed to identify the responsible physical mechanisms, but it is out of the scope of this paper and should be documented in a separate paper. In addition, within this domain that encompasses the Pacific storm track, the frequency of occurrence
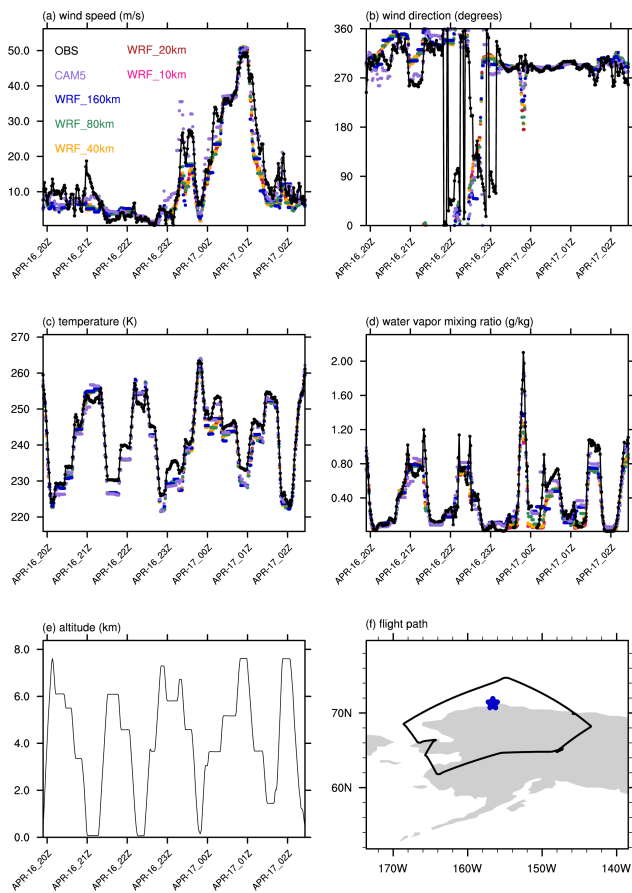
Fig. 3. The simulated and observed **(a)** wind speed $(\mathrm{m\,s^{-1}})$, **(b)** wind direction (degree), **(c)** temperature (K), and **(d)** water vapor mixing ratio $(\mathrm{g\,kg^{-1}})$ at **(e)** altitude along **(f)** the DC-8 flight path on 16 April 2008, during the ARCTAS field campaign. The blue star in **(f)** denotes the location of Barrow, Alaska (71.32° N, 156.62° W).

Fig. 4. Time series of observed and simulated **(a)** liquid water content $(\mathrm{g\,m^{-3}})$ and **(b)** ice water content $(\mathrm{g\,m^{-3}})$ and 5th, 25th, 50th, 75th, and 95th percentile of observed and simulated **(c)** liquid water content $(\mathrm{g\,m^{-3}})$ and **(d)** ice water content $(\mathrm{g\,m^{-3}})$ over all of the aircraft flights. **(e)** and **(f)** depict the altitude and flight path, respectively, of 15 Convair-580 flight paths during the ISDAC field campaign. Vertical bars in **(a)** and **(b)** show the range of the 5th and 95th percentile of the observations within each hour.

for convective clouds is found to decrease slightly with increasing resolution, from 20.7 % for the 160 km simulation to 17.6 % for the 10 km simulation, contributing 4.1 % and 2.6 % of the total cloud fraction, respectively. While CAM5 and WRF_160 km produce similar features, the remaining differences between these two simulations can be attributed to the differences in their resolutions, time steps, and dynamical cores. We have performed a sensitivity test (not shown) and found that the difference in the simulated clouds and aerosols between these two model simulations can be greatly reduced by setting the CAM5 time step (30 min) to a smaller time step (5 min) that is closer to WRF's time step (1 min). The model dependence on time step is currently under investigation and will be documented in a separate paper.

As previously mentioned, global models have difficulties simulating aerosols in the Arctic, producing a significant low bias of aerosol concentrations especially near the surface (Shindell et al., 2008). Using the same aircraft transect in Fig. 3, we show that aerosol mass concentrations of black
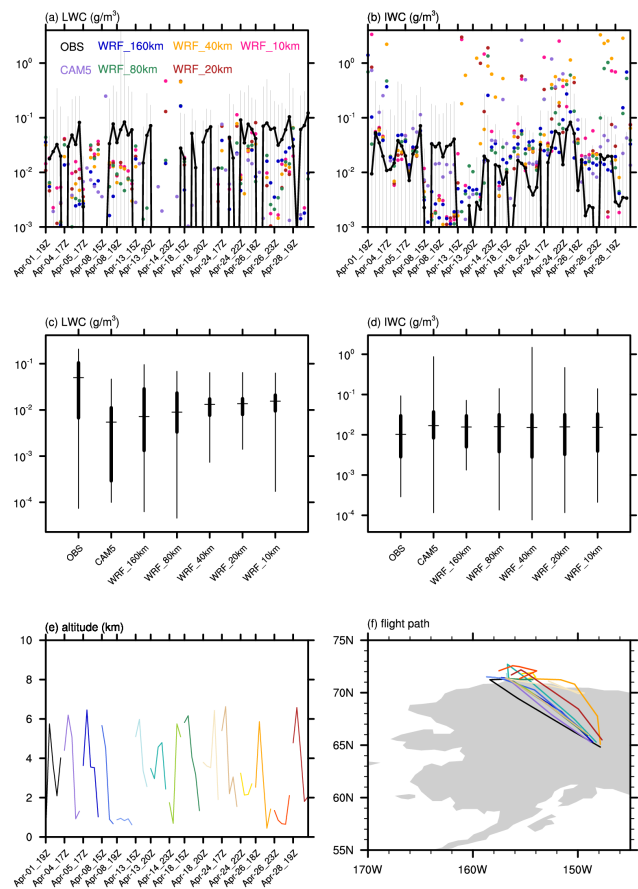
carbon, organic matter, ammonia, and sulfate are low in all model simulations by about 1 order of magnitude (Fig. 5). Model simulations also exhibit occasional drops in aerosol concentrations when the aircraft measurements are near the surface, showing 2–3 orders of magnitude lower aerosol concentrations than observations. Increasing resolution reduces the bias, but even with the smallest grid spacing of 10 km a significant bias remains. Since these aircraft measurements were taken a few days before an episode with much higher aerosol concentrations that started around 20 April, this result suggests that the model has a much lower background aerosol concentration. Meanwhile, the variability of the simulated aerosols increases with resolution because the spatially inhomogeneous distribution of aerosols is better resolved in high-resolution simulations.

Figure 6 summarizes profiles of BC concentration from a total of eight flights from the DC-8 and P3-B aircrafts
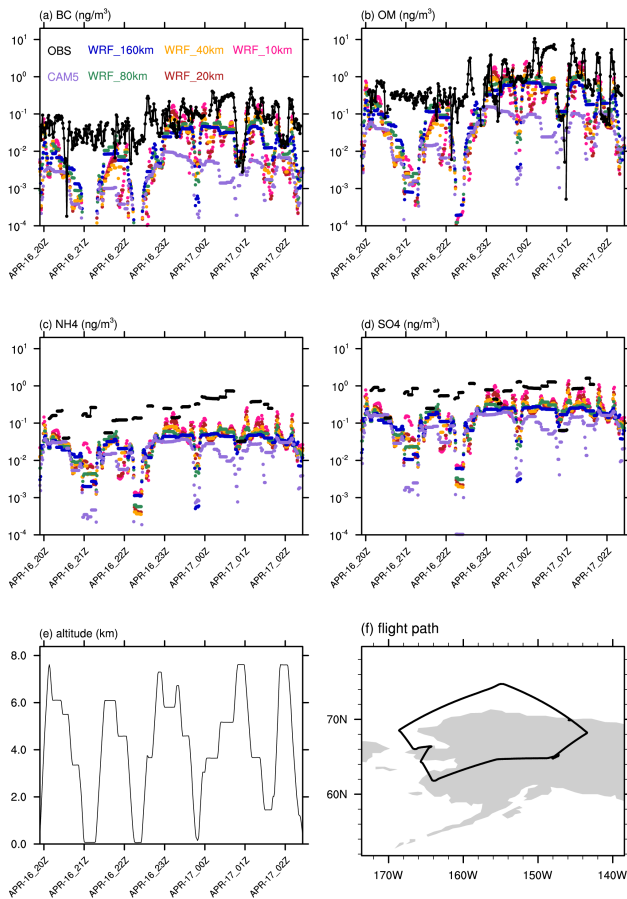
Fig. 5. The observed and simulated concentrations (ng m^{-3}) of **(a)** black carbon, **(b)** organic matter, **(c)** ammonium, and **(d)** sulfate at **(e)** altitude along **(f)** the DC-8 flight path on 16 April 2008, during the ARCTAS field campaign.

Fig. 6. Vertical profile of the observed and simulated median, 5th and 95th percentile black carbon concentration (ng m^{-3}), sampled from a total of eight P3B and DC-8 flights on 6–17 April 2008, during the ARCTAS field campaign.

taken between 6 and 17 April. This period is representative of the background aerosol state, as opposed to the high aerosol concentrations associated with transport of anthropogenic and biomass burning plumes over Alaska around 20 April. All model simulations are about 2–3 orders of magnitude too low at the surface, and about 1–2 orders of magnitude too low aloft. In general, the higher resolution model simulations show greater variability of BC concentration that results from narrower aerosol plumes with higher concentrations. The concentrations outside of the plume's centers are also lower since the low-resolution simulations tend to dilute the aerosols over a larger region. Decreasing grid spacing from the 160 to 10 km grid spacing reduces the low bias of BC at the surface by about a factor of 5. Figure 7 compares simulated surface BC concentrations at Barrow with PSAP measurements of equivalent BC (EBC) (Sharma et al., 2006) at the surface with the specific attenuation of 10 m^2 g^{-1} (S. Sharma, personal communication, 2012). The monthly mean EBC concentration is about 2–3 orders of magnitude higher than model simulations (Fig. 7a),
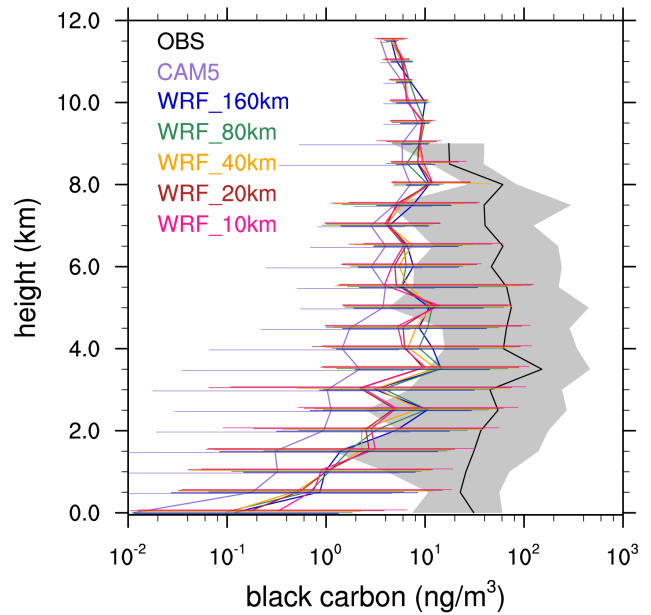
and the models consistently underpredict the background surface BC concentration by about 3–5 orders of magnitude, and by about 1–3 orders of magnitude when the episode of high BC concentration starts around 20 April when the observed BC increases from about 70 ng m^{-3} to 500 ng m^{-3}, and the model simulations also increase from about 0.1 to 50 ng m^{-3} (Fig. 7b). This model bias reduces monotonically with increasing resolution. These results show that the high-resolution simulations are able to deliver BC from the source regions over Asia to Barrow when the high BC concentration episode took place, even though all resolutions fail to produce the background BC concentration at the observed level. The low background BC might be attributed to either model deficiencies in transporting aerosols into the Arctic due to weaker eddy transport (Ma et al., 2013b) and stronger wet scavenging in the mid-latitudes (Wang et al., 2013), the underestimation or omission of aerosol sources (Stohl et al., 2013; Q. Wang et al., 2011), or a combination of both. The uncertainty associated with the emission inventory is considered to be a factor of 2 or more (Bond et al., 2004; Ramanathan and Carmichael, 2008), and its effect on the simulation requires further investigations.

Figure 8 shows snapshots of the simulated distribution of cloud fraction and BC at 00:00 UTC on 20 April. It illustrates the effect of increasing horizontal resolution. Although the domain-averaged cloud fraction from simulations of different resolutions is about the same (∼ 0.2) (Fig. 8a–f), the simulated instantaneous surface BC over Barrow (nearest model grid cell from Barrow) increases by over 1 order of
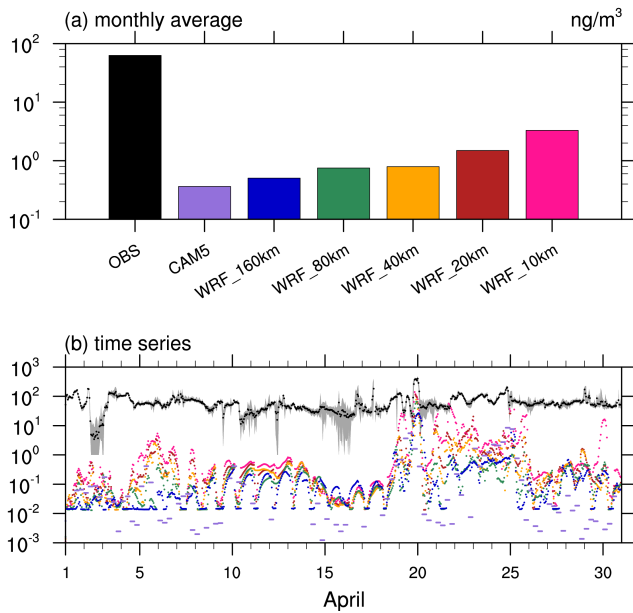
Fig. 7. Surface black carbon concentration (ng m^{-3}) over Barrow from model simulations and PSAP measurements: **(a)** monthly average and **(b)** time series.

magnitude with resolution, from 3.7 ng kg^{-1} for the 160 km grid-spacing simulation to 51.6 ng kg^{-1} for the 10 km grid-spacing simulation (Fig. 8h and l). The BC concentrations over Barrow in the high-resolution simulations averaged over the corresponding 160 km grid cell increase monotonically with increasing resolution, reaching 50.9 ng kg^{-1} in the 10 km grid-spacing simulation. The instantaneous maximum BC concentration within the corresponding 160 km grid cell over Barrow increases by about a factor of 30 (from 3.7 ng kg^{-1} to 95.6 ng kg^{-1}), suggesting that the spatial variability of BC also increases with resolution, consistent with previous studies (Gustafson Jr. et al., 2011; Qian et al., 2010). These results suggest that the unrealistic assumption of homogeneous aerosol distribution within each grid cell in CAM5 might be at least partly responsible for the underestimation of aerosol transport into the Arctic, and some of the bias that remains in the high-resolution simulations is likely due to the low values of BC present in the boundary conditions for the regional simulations delivered to the region by the low-resolution CAM simulations.

Figure 8g–l show that the large difference in surface BC concentration at Barrow is related to the filamentary structure of aerosol plumes, which can only be resolved in the high-resolution simulations, and the transport of BC from northeast Asia to Barrow is sensitive to this flow feature. In high-resolution simulations, a concentrated aerosol plume located in the gap between the clouds of two frontal systems is evident (Fig. 8f and l). Since clouds and the associated precipitation play a critical role removing aerosols in CAM5 (Liu et al., 2012; Wang et al., 2013) and the poleward transport
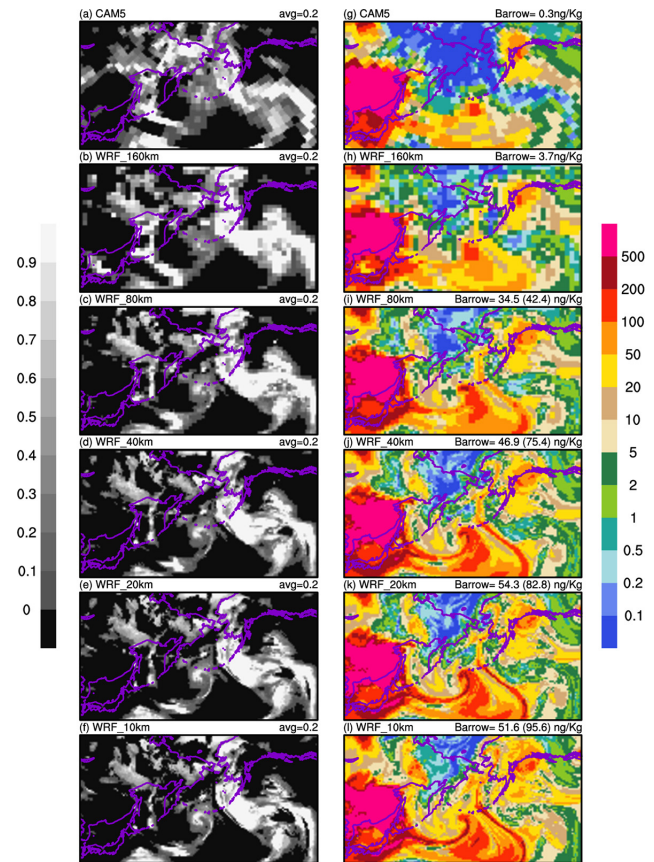

Fig. 8. The simulated **(a)**–**(f)** cloud fraction and **(g)**–**(l)** black carbon mixing ratio (ng kg^{-1}) at the second lowest model layer at 00Z of 20 April 2008. Numbers in **(a)**–**(f)** are the domain average cloud fraction. In **(g)**–**(l)**, black carbon mixing ratios at the second lowest model over Barrow are given, and numbers in parentheses are the maximum black carbon concentration within the 160 km cell over Barrow.

of aerosols in these latitudes depends on features driven by these eddies (Ma et al., 2013b), this cloudless transport pathway between two mesoscale eddies facilitates the transport of aerosols into the Arctic. In low-resolution simulations, the coarse grids are unable to resolve these filamentary features associated with mesoscale eddies; hence, aerosols are subject to wet removal within clouds along the path.

All six aerosol species in MAM3 show behavior similar to BC (Fig. 9) with more aerosols delivered to the Arctic (north of 66.5° N) with increasing resolution, and the effect gradually accumulates over time. The 10 km model simulation appears to show a much larger increase of aerosol burdens over other simulations. The transport of sea salt aerosols into the Arctic shows the largest sensitivity to resolution for this domain. One possible explanation is that the resolution-dependent cloud-free pathways are more frequent over ocean than land in the simulations. Hence, the impact of the cloud-free pathways (where aerosols are not subject to cloud processing) is greatest for aerosols produced
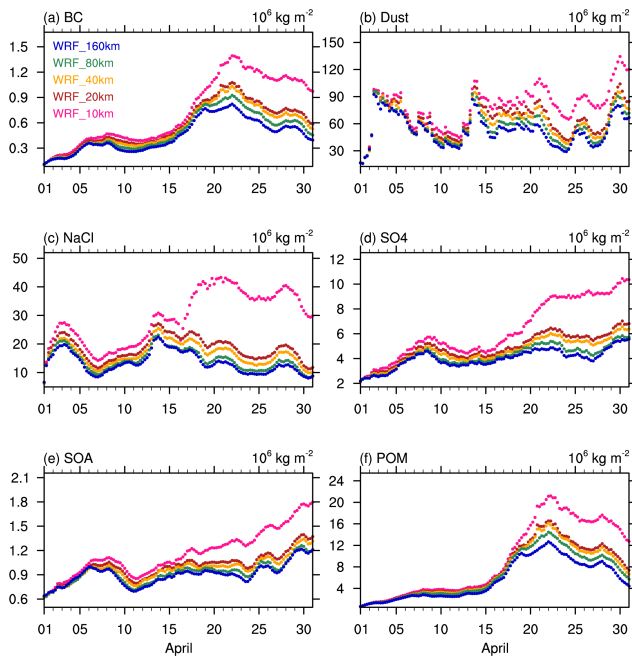
Fig. 9. Time series of total column burden of **(a)** black carbon, **(b)** mineral dust, **(c)** sea salt, **(d)** sulfate, **(e)** secondary organic aerosol, and **(f)** primary organic matter (10^6 kg m^{-2}) in the Arctic (north of $66.5°$ N).

Fig. 10. Cloud susceptibility to aerosol forcing as a function of model horizontal grid spacing.

over ocean. Another possible explanation is that the sea salt aerosols have a source that is not remote in the regional simulations, so it is not dependent on the boundary conditions. Although sea salt emission would generally be sensitive to surface wind speeds, and thus could have a resolution dependence (higher wind speeds being resolved with smaller grid spacings), this effect is not present in our simulation because the sea salt emissions have been prescribed from CAM5 for all the WRF-Chem simulations.

As aerosol and cloud distributions and loadings evolve, the aerosol–cloud interactions may change accordingly. One convenient means of characterizing the relationship between aerosols and clouds is "cloud susceptibility to aerosols", defined as the fractional increase of cloud LWP to fractional increase of AOT (e.g., Quaas et al., 2009; M. Wang et al., 2011), often expressed as the slope of a measure of fractional change in a cloud property related to its radiative effect (in this case using liquid water column burden) to fractional change in aerosol amount (in this case using the AOT). CAM5 has a very high value of susceptibility (Wang et al., 2012), and part of this behavior can be attributed to parametric uncertainty (Liu et al., 2014). Figure 10 displays the susceptibility, calculated from hourly model output of AOT and LWP for the whole simulation period at every grid point over the entire domain (excluding the buffer zone of the lateral boundary), as a function of horizontal resolution. The cloud susceptibility to aerosols decreases by about 45 % in the highest-resolution simulation. The WRF_10 km
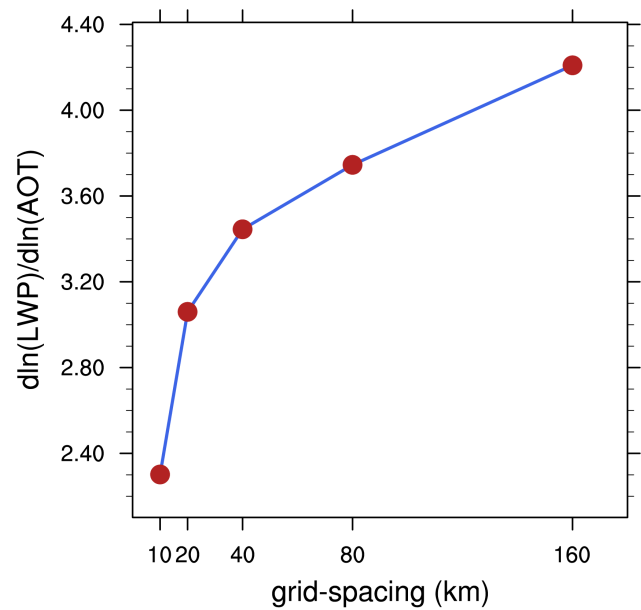
simulation shows much lower cloud susceptibility, which leads to weaker scavenging and results in larger aerosol burdens and higher long-range transport of aerosols as shown in Fig. 9. The reduction of cloud susceptibility with increasing resolution can be largely explained by the fact that aerosol plumes and clouds are less collocated in high-resolution simulations as shown in Fig. 8. Clouds and precipitation occur in narrower spatial regions, and the occurrence of clouds and precipitation in any given model column is less frequent in many columns, producing weaker aerosol–cloud interactions. Other physical mechanisms may also be sensitive to resolution (e.g., autoconversion and accretion) and affect cloud susceptibility and aerosol indirect forcing. These issues are being explored and will form the basis of a later study.

6 Comparison of the CAM5 physics with a common WRF parameterization suite

The previous section demonstrated the behavior of aerosols and clouds in the CAM5 physics suite by tightly constraining the meteorological component of the simulations to observations through nudging. In this section, we use "freely evolving" simulations of the WRF-Chem model using the CAM5 physics suite (labeled as "WRF_CAM5") and a commonly used parameterization suite within the WRF-Chem mesoscale modeling community (labeled as "WRF_MESO") to expose differences in the two different physics packages. These simulations indicate where the parameterizations used by the global and mesoscale modeling communities are
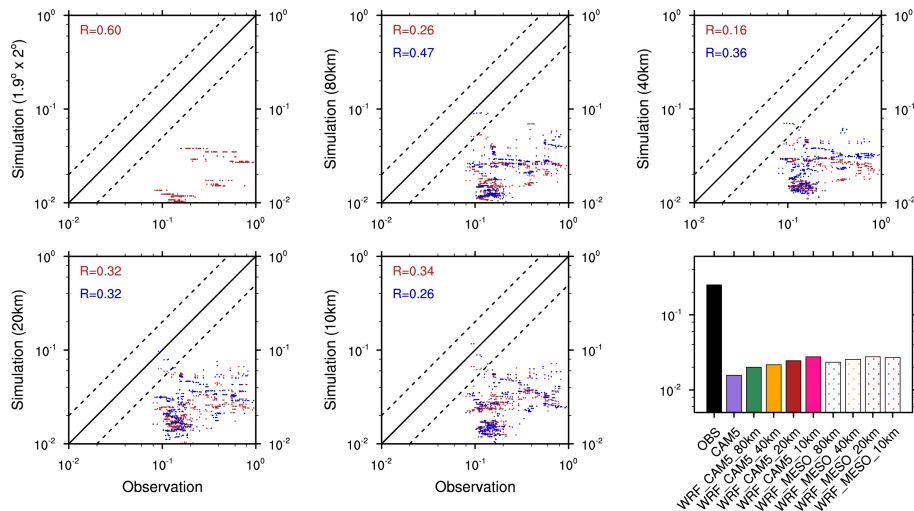
Fig. 11. Scatterplots of aerosol optical thickness from model simulations that utilize the CAM5 (red) and WRF (blue) physics suite, evaluated against AERONET observations at Barrow (71.31° N, 156.67° W) and Bonanza Creek (64.74° N, 148.32° W).

significantly different, and provide an opportunity to quantify the performance of alternative process modules before they are incorporated and used by global climate models. Such a comparison could be expanded to provide insights into the model's structural uncertainty (deficiencies associated with specific treatments of various physical and chemical processes in the model parameterizations) and help to identify the components that produce the largest differences in simulations by changing process representations one at a time. For brevity, we restrict our analysis to a demonstration of capability rather than quantifying effects of each process in the two different parameterization suites.

The WRF_MESO configuration includes a double moment cloud microphysics scheme (Morrison et al., 2009), the Grell and Devenyi (2002) cumulus ensemble parameterization, an operational boundary layer scheme for the Eta model (Janjic, 2002) that employs a turbulent kinetic energy formulation (Mellor and Yamada, 1982), the Noah land surface model (Chen and Dudhia, 2001), and the 8-size bin version of Model for Simulating Aerosol Interactions and Chemistry (MOSAIC) aerosol model (Zaveri et al., 2008). The WRF_MESO configuration does not treat aerosol wet removal and vertical transport by subgrid convective clouds, but does represent wet removal when the cell-averaged values indicate clouds are present, and aerosols undergo vertical transport by resolved winds and turbulent processes. Our analysis later in this section shows that these differences do not contribute to large differences in the simulations over this high-latitude domain. Both model configurations are run at multiple grid spacings: 80, 40, 20, and 10 km (labeled as "WRF_CAM5_80 km", "WRF_ CAM5_40 km", "WRF_CAM5_20 km", "WRF_ CAM5_10 km", "WRF_MESO_80 km", "WRF_MESO_ 40 km", "WRF_MESO_20 km", and "WRF_MESO_

10 km"). We performed the evaluation within a smaller domain that encompasses Alaska and its vicinity (area enclosed by purple lines in Fig. 12f), approximately 3000 km by 3000 km in total area. All WRF simulations use the global CAM5 results for the initial and boundary conditions for model state (meteorology, cloud condensate, aerosols, and trace gases). The same emission inventory is used to drive all model simulations. The MAM3 aerosol concentrations and emissions from CAM5 are mapped to the corresponding MOSAIC aerosol species in the emission interface subroutine as well as the initial and boundary conditions of WRF_MESO simulations. While the WRF-Chem model with the CAM5 physics suite uses prescribed sea salt and dust emissions as well as surface moisture and heat fluxes archived from the offline CAM5 simulation, the WRF_MESO simulations compute these fields as a function of surface wind speed.

Figure 11 shows that when driven by the same initial and boundary conditions from the CAM5 simulation, all the WRF_CAM5 and WRF_MESO simulations underpredict AOT by 1 order of magnitude compared to AERONET observations at Barrow and Bonanza Creek. Increasing resolution only has a very modest improvement, and the WRF_CAM5 and WRF_MESO simulations produce similar results. Vertical profiles are also similar between model configurations, and all simulations are biased low by 1 order of magnitude near the surface compared with the observations calculated from the samples obtained from the ARCPAC field campaign (Fig. 12, and see Koch et al., 2009, for details on data processing).

Local emissions have been suggested to have a very large contribution efficiency to the aerosol concentrations in the Arctic (Ma et al., 2013a; Stohl et al., 2013). However, they are underestimated in the POLMIP emission inventory, and
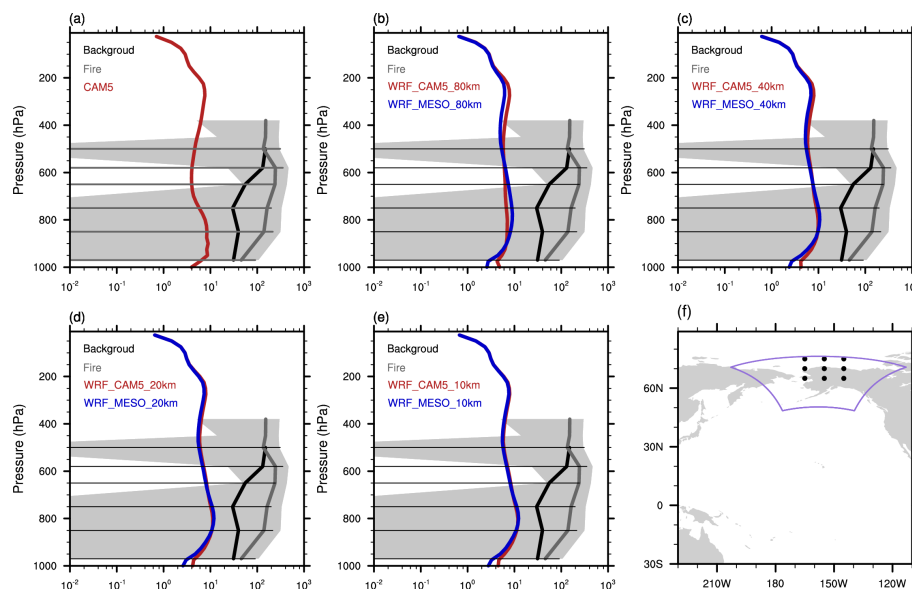
Fig. 12. Monthly mean vertical profiles of BC mixing ratio (ng kg^{-1}) from model simulations that uses the CAM5 (red) or WRF (blue) physics suite, compared with observations from the ARCPAC field campaign (dotted area). The purple line encloses the area of the WRF domain.

most aerosols in the Arctic originate from remote sources (Ma et al., 2013a) and enter this WRF domain through the lateral boundary conditions. Since aerosol concentrations in the coarse-resolution CAM5 simulation are significantly underestimated (Ma et al., 2013b; Wang et al., 2013) due to a combination of strong wet scavenging over the ocean and weaker eddy transport in the low-resolution CAM5 simulation, and underestimation of emissions of aerosols and their precursors, the regional WRF simulations receives low aerosol inflows from the model's western boundary over Bering Sea and southern boundary over the Pacific Ocean, leading to a low bias for aerosol concentrations and AOT. In addition, since the aerosol plumes reaching this region are already aged, different treatments of aerosol chemistry between MAM3 and MOSAIC have only marginal effects on the simulation. For regional domains containing a major source region where local emissions dominate and aerosols are less aged, differences between MAM3 and MOSAIC can lead to significantly different aerosol simulations (not shown).

In spite of the strong influence from the lateral boundaries, there is still one noticeable difference between WRF_CAM5 and WRF_MESO: BC concentration near the surface is about a factor of 2 higher in the WRF_CAM5 simulations (Fig. 12). One possible explanation contributing to this difference is that the CAM5 physics suite takes into account the resuspension of aerosol particles from evaporated raindrops, which is omitted in the WRF_MESO physics suite. Note that both the WRF_CAM5 and the WRF_MESO physics suite consider the aerosol resuspension process in decaying clouds (when cloud droplets evaporate). Further investigation is needed to

understand all differences between the two parameterizations and their effects on the simulation, and this modeling framework can be useful for such process-level studies.

The simulated total column water vapor and precipitation rates in all model simulations are generally in good agreements with observations with high correlations and small biases (Figs. 13 and 14). All model simulations overpredict precipitation when the observed precipitation is light but do much better for rain amounts above about 0.4 mm day^{-1}. The correlation between model simulations and GPCP precipitation rate is very good for rain rates larger than 0.4 mm day^{-1} and poor below that. Increasing resolution generally has little effect on the daily precipitation in this high-latitude domain that is largely over land. However, resolution dependence is expected for instantaneous precipitation rates and precipitation over regions where synoptic and mesoscale features of moisture convergence are better resolved at higher resolution.

Figure 15 shows that the WRF_CAM5 simulations produce higher in-cloud liquid water condensate amount and much more realistic frequency of occurrence of liquid cloud than the WRF_MESO simulations, compared with ARM observations at Barrow. The cloud statistics within cloudy cells in all model simulations are qualitatively similar and in good agreement with observations, but WRF_CAM5 simulations exhibit some high in-cloud LWP events when the liquid cloud fraction is small and/or raindrops are at present (Fig. 16). One possible explanation for this difference is that the CAM5 physics suite considers subgrid clouds, which allows clouds to form within a fraction of the grid box even if the whole grid box is not saturated. Gustafson Jr.
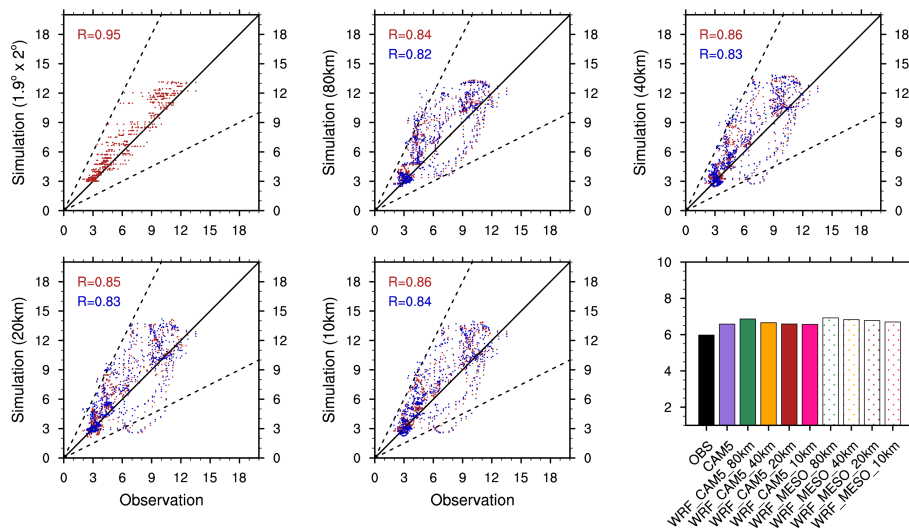
Fig. 13. Scatterplots of total column precipitable water vapor ($g\,m^{-2}$) from model simulations that utilize the CAM5 (red) and WRF (blue) physics suite evaluated against the ARM best estimates at Barrow.
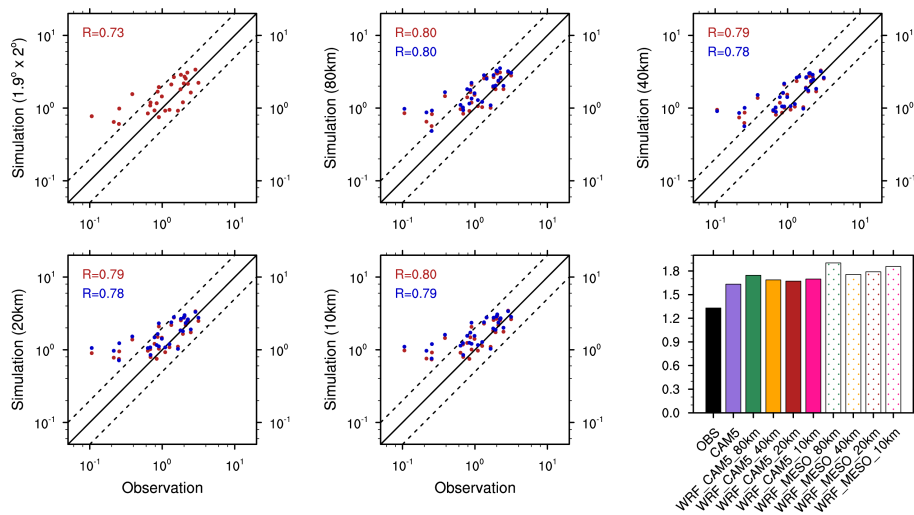

Fig. 14. Scatterplots of the domain mean daily precipitation rate ($mm\,day^{-1}$) from model simulations that utilize the CAM5 (red) and WRF (blue) physics suite evaluated against the GPCP daily data averaged over the same domain.

et al. (2013) reached a similar conclusion that omitting the treatment of subgrid cloud in WRF running with CAM5 physics suite for typical mesoscale resolutions (grid spacing ranging from 4 to 32 km) results in a reduction of liquid and ice condensate amount. In addition, Fig. 15 also shows that the WRF_CAM5 simulations produce low liquid water condensate above 1.5 km compared with observations, and the bias is improved with increasing resolution. In contrast, the WRF_MESO simulations do not show the same behavior. This model bias could be attributed to the model representation of ice cloud processes and rainwater treatment. For example, different rainwater treatment between the Morrison et al. (2009) scheme used in WRF_MESO simulations and the Morrison and Gettelman (2008) scheme used

in WRF_CAM5 simulations can produce different clouds because the emphasis of rain production can be shifted from autoconversion to accretion as the model changes its rainwater treatment from diagnostic rain (as used in the WRF_CAM5 cloud microphysics) to prognostic rain (as used in the WRF_MESO cloud microphysics), which reduces the aerosol effect on clouds (Posselt and Lohmann, 2009). Quantification of the effect of each process in the two parameterizations is beyond the scope of this study and should be addressed by an independent study.

Figure 17 shows that all model simulations produce lower ice water condensate amount and higher frequency of occurrence of ice clouds compared to observations, and the WRF_CAM5 simulations agree better with observations than
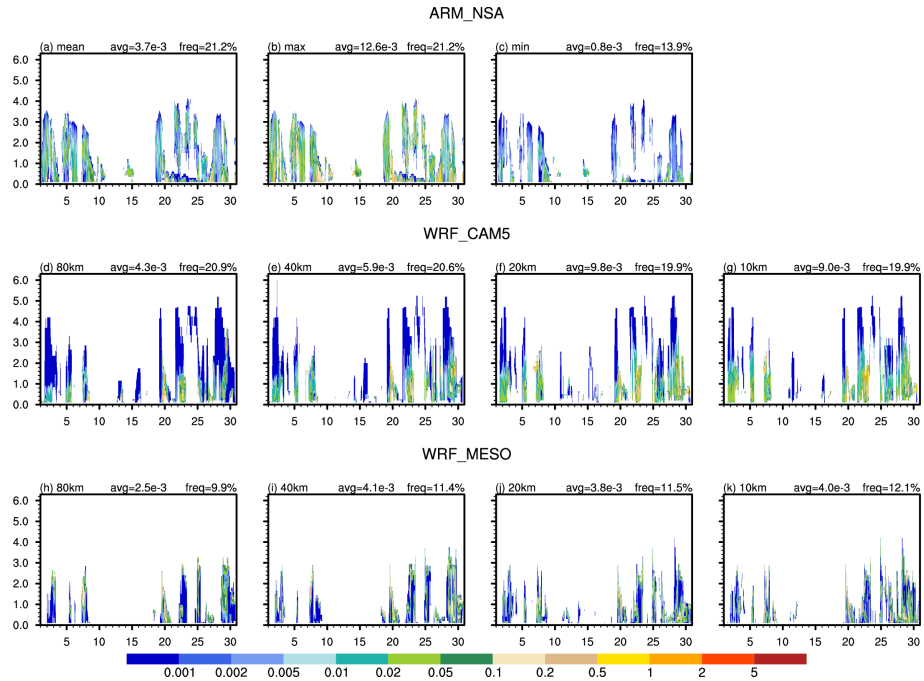
Fig. 15. Time series of vertical profiles of liquid water content ($g\,kg^{-1}$) from ARM: **(a)** hourly mean, **(b)** hourly maximum, and **(c)** hourly minimum, compared with the in-cloud liquid water content ($g\,kg^{-1}$) from **(d)**–**(g)** WRF_CAM5 and **(h)**–**(k)** WRF_MESO simulations at Barrow. Values of average liquid water content and frequency of occurrence of liquid cloud are given.
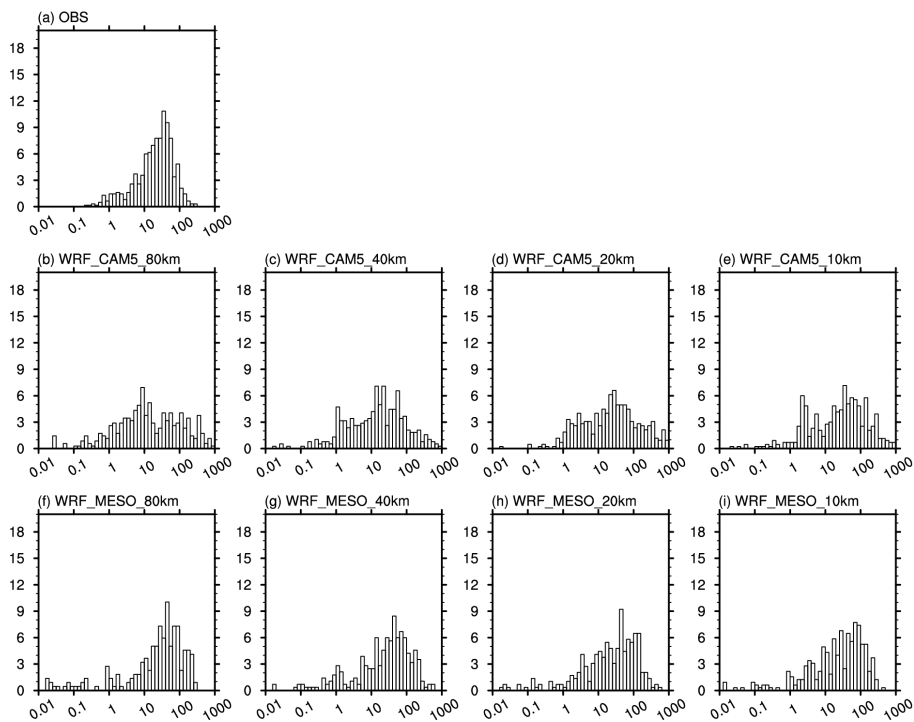

Fig. 16. Histograms (percentage) of **(a)** the observed liquid water path ($g\,m^{-2}$) from ARM Cloud Retrieval Ensemble Dataset, and **(b)**–**(i)** the simulated in-cloud liquid water path ($g\,m^{-2}$) from **(b)**–**(e)** WRF_CAM5 and **(f)**–**(i)** WRF_MESO simulations at Barrow.
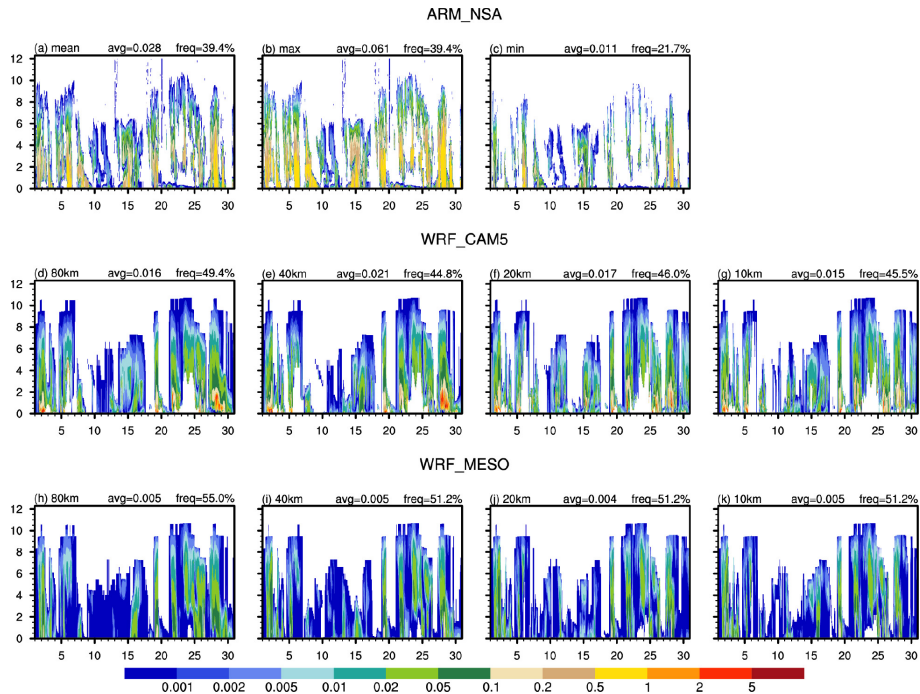
Fig. 17. Time series of vertical profiles of ice water content ($g\,kg^{-1}$) from ARM: **(a)** hourly mean, **(b)** hourly maximum, and **(c)** hourly minimum, compared with the in-cloud ice water content ($g\,kg^{-1}$) from **(d)**–**(g)** WRF_CAM5 and **(h)**–**(k)** WRF_MESO simulations at Barrow. Values of average ice water content and frequency of occurrence of ice cloud are given.
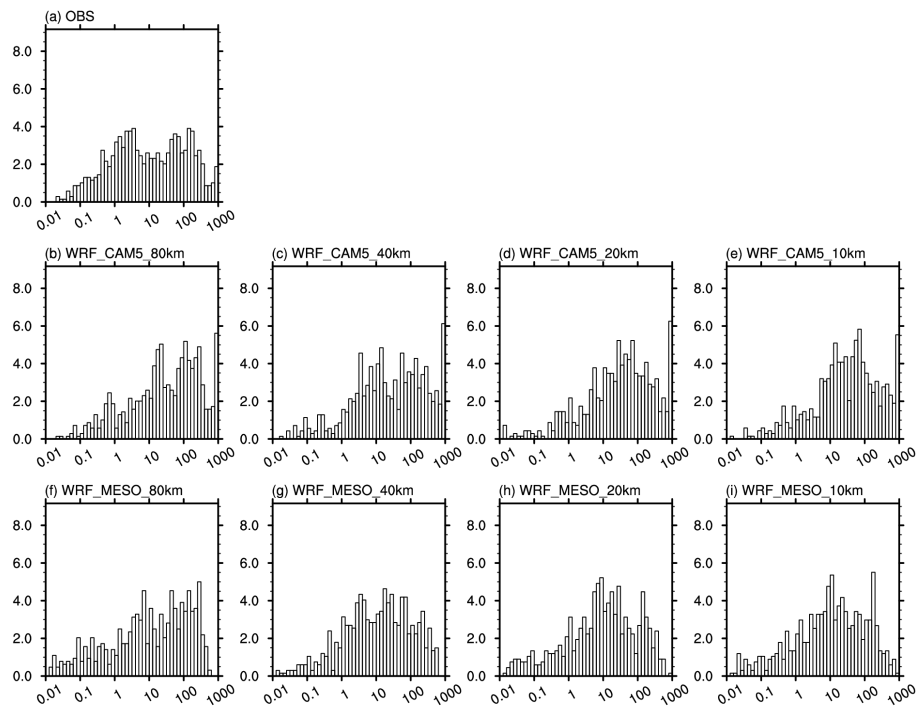

Fig. 18. Histograms (percentage) of **(a)** the observed ice water path ($g\,m^{-2}$) from ARM Cloud Retrieval Ensemble Dataset, and **(b)**–**(i)** the simulated in-cloud ice water path ($g\,m^{-2}$) from **(b)**–**(e)** WRF_CAM5 and **(f)**–**(i)** WRF_MESO simulations at Barrow.

the WRF_MESO simulations in terms of both frequency of occurrence and monthly mean in-cloud ice water content. The in-cloud ice water path distributions between model simulations and observations are qualitatively similar, but the WRF_CAM5 simulations show more events of high ice water path, whereas the WRF_MESO simulations have more low ice water path events (Fig. 18). The distributions of the frequency of occurrence for both ice and liquid clouds are found insensitive to model resolution. In addition, the observations show a mean liquid-to-total water ratio of about 29.8 % in mixed phase clouds, higher than the WRF_CAM5 simulations (increasing from 13.4 % to 25.3 % with resolution) and lower than the WRF_MESO simulations (increasing from 40.4 % to 46.3 % with resolution). These differences highlight sensitivity to the different representations of ice cloud processes between the two cloud microphysics parameterizations. For example, while the Morrison et al. (2009) scheme treats the Wegener–Bergeron–Findeisen process explicitly by computing both the evaporation of liquid condensates and the deposition of water vapor in mixed phase clouds using cell-averaged quantities, the Morrison and Gettelman (2008) parameterization computes the deposition rate by converting the subgrid in-cloud liquid to ice condensates directly. This difference can lead to different ice deposition rates. Insights into the improvement on the ice cloud parameterization could be gained from further investigation.

In summary, this modeling framework can be useful to probe effects of different parameterizations. We demonstrated that the CAM5 physics suite in WRF-Chem produces a realistic regional meteorology and aerosol distributions similar to simulations using a common set of the WRF parameterizations. Some improvements in the BC concentration near the surface, the frequency of occurrence of liquid water content, and the ice water condensate amount were produced by the CAM5 physics suite. However, the underestimation of aerosols in the global model remains in the RCM. The low bias is insensitive to model resolutions and physics suites for this particular domain and the simulated period of time in this study, suggesting that much of the underestimation is caused by the low estimates of local emissions in this emission inventory and the low concentrations of BC entering the region from the boundary condition values provided by CAM5.

7 Concluding remarks

The CAM5 physics parameterization suite has been recently ported to the WRF-Chem model. A downscaling modeling framework has been developed that minimizes inconsistencies between the global and regional models. This allows us to run the CAM5 physics suite over a range of scales. We use this downscaling modeling framework to evaluate the CAM5 physics at high resolution and to directly compare model predictions with high-resolution field campaign data. The suite

was released as part of WRF (and WRF-Chem) version 3.5 in April 2013 for broader use by both the WRF and CAM communities for various research objectives. This manuscript describes how the CAM5 parameterizations were implemented in WRF-Chem and provides an initial evaluation.

We ported the CAM5 physics suite in WRF using interface routines to minimize changes to the CAM5 codes (both formulation and programming). This approach (1) eases implementation of future updates, (2) minimizes the likelihood of changing the behavior of the parameterizations because of implementation issues, and (3) makes the CAM5 physics suite behave similarly in WRF and CAM when running at similar resolutions. Necessary minor modifications appear to have only marginal effects on the simulation. We extended the capabilities of WRF by adding parameterizations that are designed for larger space and timescales, and provided a means to compare simulations using different parameterizations within the same modeling framework to better assess the effects of different model treatments of aerosols, clouds, convections, and aerosol–cloud interactions. The new parameterization suite supports a consistent treatment of subgrid-scale clouds, a feature that was previously neglected in WRF and WRF-Chem.

We demonstrated the use of this downscaling modeling framework by exploring the resolution dependence of the CAM5 physics suite for one test-bed case. Some model biases in CAM5 (e.g., low aerosol concentration near the surface in the Arctic and high cloud susceptibility to aerosols) were found to reduce with increasing horizontal resolution without any modification to the model physics. While cloud distributions become more realistic at higher resolution as expected, the domain averages of some cloud properties (liquid and ice water path, precipitation rate, etc.) were not very sensitive to varying horizontal grid spacing using the CAM5 physics suite. Our analysis shows that the collocation of aerosols and clouds is very different at different model resolutions, resulting in differences in long-range aerosol transport and cloud susceptibility to aerosols. At higher-resolutions, filamentary aerosol transport pathways evolve according to the circulation associated with the resolved mesoscale eddies that are not present at low resolution. This feature leads to a significant increase of aerosol concentration over the Arctic due to greater eddy transport and weaker wet scavenging (resulting from changes in the frequency of occurrence of clouds, precipitation, and the collocation of clouds and aerosols) during transport. We also show that the WRF-Chem model running with the CAM5 physics suite produces realistic meteorological conditions over the high-latitude domain, and yields higher liquid and ice water condensate simulations and higher BC concentrations near the surface than the example WRF physics suite we examined. We believe this framework can be used to guide future parameterization development that improves the representation of aerosol, cloud, and aerosol–cloud interaction processes and their subgrid variability. However, the present

study focuses on only one case, and there are many parameterization choices in WRF; other parameterization combinations are likely to perform differently for this test-bed case as well as in other regions/seasons. Additional analyses and more case studies are needed to understand the overall performance of the CAM5 physics compared to other model treatments.

References

Abdul-Razzak, H. and Ghan, S. J.: A parameterization of aerosol activation 2. Multiple aerosol types, J. Geophys. Res.-Atmos., 105, 6837–6844, doi:10.1029/1999jd901161, 2000.

Barnard, J. C., Fast, J. D., Paredes-Miranda, G., Arnott, W. P., and Laskin, A.: Technical Note: Evaluation of the WRF-Chem "Aerosol Chemical to Aerosol Optical Properties" Module using data from the MILAGRO campaign, Atmos. Chem. Phys., 10, 7325–7340, doi:10.5194/acp-10-7325-2010, 2010.

Bond, T. C., Streets, D. G., Yarber, K. F., Nelson, S. M., Woo, J. H., and Klimont, Z.: A technology-based global inventory of black and organic carbon emissions from combustion, J. Geophys. Res.-Atmos., 109, D14203, doi:10.1029/2003jd003697, 2004.

Bretherton, C. S. and Park, S.: A New Moist Turbulence Parameterization in the Community Atmosphere Model, J. Climate, 22, 3422–3448, doi:10.1175/2008jcli2556.1, 2009.

Brock, C. A., Cozic, J., Bahreini, R., Froyd, K. D., Middlebrook, A. M., McComiskey, A., Brioude, J., Cooper, O. R., Stohl, A., Aikin, K. C., de Gouw, J. A., Fahey, D. W., Ferrare, R. A., Gao, R.-S., Gore, W., Holloway, J. S., HÜbler, G., Jefferson, A., Lack, D. A., Lance, S., Moore, R. H., Murphy, D. M., Nenes, A., Novelli, P. C., Nowak, J. B., Ogren, J. A., Peischl, J., Pierce, R. B., Pilewskie, P., Quinn, P. K., Ryerson, T. B., Schmidt, K. S., Schwarz, J. P., Sodemann, H., Spackman, J. R., Stark, H.,

Thomson, D. S., Thornberry, T., Veres, P., Watts, L. A., Warneke, C., and Wollny, A. G.: Characteristics, sources, and transport of aerosols measured in spring 2008 during the aerosol, radiation, and cloud processes affecting Arctic Climate (ARCPAC) Project, Atmos. Chem. Phys., 11, 2423–2453, doi:10.5194/acp-11-2423-2011, 2011.

Caya, D. and Biner, S.: Internal variability of RCM simulations over an annual cycle, Clim. Dynam., 22, 33–46, doi:10.1007/S00382-003-0360-2, 2004.

Chen, F. and Dudhia, J.: Coupling an advanced land surface-hydrology model with the Penn State-NCAR MM5 modeling system. Part I: Model implementation and sensitivity, Mon. Weather Rev., 129, 569–585, doi:10.1175/1520-0493(2001)129<0569:Caalsh>2.0.Co;2, 2001.

Chou, C., Chiang, J. C. H., Lan, C. W., Chung, C. H., Liao, Y. C., and Lee, C. J.: Increase in the range between wet and dry season precipitation, Nat. Geosci., 6, 263–267, doi:10.1038/Ngeo1744, 2013.

Cubison, M. J., Ortega, A. M., Hayes, P. L., Farmer, D. K., Day, D., Lechner, M. J., Brune, W. H., Apel, E., Diskin, G. S., Fisher, J. A., Fuelberg, H. E., Hecobian, A., Knapp, D. J., Mikoviny, T., Riemer, D., Sachse, G. W., Sessions, W., Weber, R. J., Weinheimer, A. J., Wisthaler, A., and Jimenez, J. L.: Effects of aging on organic aerosol from open biomass burning smoke in aircraft and laboratory studies, Atmos. Chem. Phys., 11, 12049–12064, doi:10.5194/acp-11-12049-2011, 2011.

Dee, D. P., Uppala, S. M., Simmons, A. J., Berrisford, P., Poli, P., Kobayashi, S., Andrae, U., Balmaseda, M. A., Balsamo, G., Bauer, P., Bechtold, P., Beljaars, A. C. M., van de Berg, L., Bidlot, J., Bormann, N., Delsol, C., Dragani, R., Fuentes, M., Geer, A. J., Haimberger, L., Healy, S. B., Hersbach, H., Holm, E. V., Isaksen, L., Kallberg, P., Kohler, M., Matricardi, M., McNally, A. P., Monge-Sanz, B. M., Morcrette, J. J., Park, B. K., Peubey, C., de Rosnay, P., Tavolato, C., Thepaut, J. N., and Vitart, F.: The ERA-Interim reanalysis: configuration and performance of the data assimilation system, Q. J. Roy. Meteorol. Soc., 137, 553–597, doi:10.1002/Qj.828, 2011.

Dentener, F., Kinne, S., Bond, T., Boucher, O., Cofala, J., Generoso, S., Ginoux, P., Gong, S., Hoelzemann, J. J., Ito, A., Marelli, L., Penner, J. E., Putaud, J.-P., Textor, C., Schulz, M., van der Werf, G. R., and Wilson, J.: Emissions of primary aerosol and precursor gases in the years 2000 and 1750 prescribed data-sets for AeroCom, Atmos. Chem. Phys., 6, 4321–4344, doi:10.5194/acp-6-4321-2006, 2006.

Deser, C., Phillips, A. S., Tomas, R. A., Okumura, Y. M., Alexander, M. A., Capotondi, A., Scott, J. D., Kwon, Y. O., and Ohba, M.: ENSO and Pacific Decadal Variability in the Community Climate System Model Version 4, J. Climate, 25, 2622–2651, doi:10.1175/Jcli-D-11-00301.1, 2012.

de Villiers, R. A., Ancellet, G., Pelon, J., Quennehen, B., Schwarzenboeck, A., Gayet, J. F., and Law, K. S.: Airborne measurements of aerosol optical properties related to early spring transport of mid-latitude sources into the Arctic, Atmos. Chem. Phys., 10, 5011–5030, doi:10.5194/acp-10-5011-2010, 2010.

Emmons, L. K., Walters, S., Hess, P. G., Lamarque, J.-F., Pfister, G. G., Fillmore, D., Granier, C., Guenther, A., Kinnison, D., Laepple, T., Orlando, J., Tie, X., Tyndall, G., Wiedinmyer, C., Baughcum, S. L., and Kloster, S.: Description and evaluation of the Model for Ozone and Related chemical Tracers, version 4

(MOZART-4), Geosci. Model Dev., 3, 43–67, doi:10.5194/gmd-3-43-2010, 2010.

Fan, J. W., Ghan, S., Ovchinnikov, M., Liu, X. H., Rasch, P. J., and Korolev, A.: Representation of Arctic mixed-phase clouds and the Wegener-Bergeron-Findeisen process in climate models: Perspectives from a cloud-resolving study, J. Geophys. Res.-Atmos., 116, D00t07, doi:10.1029/2010jd015375, 2011.

Fast, J. D., Gustafson, W. I., Easter, R. C., Zaveri, R. A., Barnard, J. C., Chapman, E. G., Grell, G. A., and Peckham, S. E.: Evolution of ozone, particulates, and aerosol direct radiative forcing in the vicinity of Houston using a fully coupled meteorology-chemistry-aerosol model, J. Geophys. Res.-Atmos., 111, D21305, doi:10.1029/2005jd006721, 2006.

Fast, J. D., Gustafson, W. I., Chapman, E. G., Easter, R. C., Rishel, J. P., Zaveri, R. A., Grell, G. A., and Barth, M. C.: The Aerosol Modeling Testbed a Community Tool to Objectively Evaluate Aerosol Process Modules, B. Am. Meteorol. Soc., 92, 343–360, doi:10.1175/2010bams2868.1, 2011.

Fuelberg, H. E., Harrigan, D. L., and Sessions, W.: A meteorological overview of the ARCTAS 2008 mission, Atmos. Chem. Phys., 10, 817–842, doi:10.5194/acp-10-817-2010, 2010.

Ganguly, D., Rasch, P. J., Wang, H. L., and Yoon, J. H.: Climate response of the South Asian monsoon system to anthropogenic aerosols, J. Geophys. Res.-Atmos., 117, D13209, doi:10.1029/2012jd017508, 2012a.

Ganguly, D., Rasch, P. J., Wang, H. L., and Yoon, J. H.: Fast and slow responses of the South Asian monsoon system to anthropogenic aerosols, Geophys. Res. Lett., 39, L18804, doi:10.1029/2012gl053043, 2012b.

Gent, P. R. and Danabasoglu, G.: Response to Increasing Southern Hemisphere Winds in CCSM4, J. Climate, 24, 4992–4998, doi:10.1175/Jcli-D-10-05011.1, 2011.

Gettelman, A., Morrison, H., and Ghan, S. J.: A new two-moment bulk stratiform cloud microphysics scheme in the community atmosphere model, version 3 (CAM3). Part II: Single-column and global results, J. Climate, 21, 3660–3679, doi:10.1175/2008jcli2116.1, 2008.

Gettelman, A., Kay, J. E., and Shell, K. M.: The Evolution of Climate Sensitivity and Climate Feedbacks in the Community Atmosphere Model, J. Climate, 25, 1453–1469, doi:10.1175/Jcli-D-11-00197.1, 2012.

Ghan, S. J. and Easter, R. C.: Impact of cloud-borne aerosol representation on aerosol direct and indirect effects, Atmos. Chem. Phys., 6, 4163–4174, doi:10.5194/acp-6-4163-2006, 2006.

Ghan, S. J., Leung, L. R., Easter, R. C., and Abdul-Razzak, K.: Prediction of cloud droplet number in a general circulation model, J. Geophys. Res.-Atmos., 102, 21777–21794, doi:10.1029/97jd01810, 1997.

Ghan, S. J., Leung, L. R., and McCaa, J.: A comparison of three different modeling strategies for evaluating cloud and radiation parameterizations, Mon. Weather Rev., 127, 1967–1984, doi:10.1175/1520-0493(1999)127<1967:Acotdm>2.0.Co;2, 1999.

Ghan, S. J., Liu, X., Easter, R. C., Zaveri, R., Rasch, P. J., Yoon, J. H., and Eaton, B.: Toward a Minimal Representation of Aerosols in Climate Models: Comparative Decomposition of Aerosol Direct, Semidirect, and Indirect Radiative Forcing, J. Climate, 25, 6461–6476, doi:10.1175/Jcli-D-11-00650.1, 2012.

Ginoux, P., Chin, M., Tegen, I., Prospero, J. M., Holben, B., Dubovik, O., and Lin, S. J.: Sources and distributions of dust aerosols simulated with the GOCART model, J. Geophys. Res.-Atmos., 106, 20255–20273, doi:10.1029/2000jd000053, 2001.

Giorgi, F. and Bi, X. Q.: A study of internal variability of a regional climate model, J. Geophys. Res.-Atmos., 105, 29503–29521, doi:10.1029/2000jd900269, 2000.

Giorgi, F. and Marinucci, M. R.: An investigation of the sensitivity of simulated precipitation to model resolution and its implications for climate studies, Mon. Weather Rev., 124, 148–166, doi:10.1175/1520-0493(1996)124<0148:Aiotso>2.0.Co;2, 1996.

Granier, C., Bessagnet, B., Bond, T., D'Angiola, A., van der Gon, H. D., Frost, G. J., Heil, A., Kaiser, J. W., Kinne, S., Klimont, Z., Kloster, S., Lamarque, J. F., Liousse, C., Masui, T., Meleux, F., Mieville, A., Ohara, T., Raut, J. C., Riahi, K., Schultz, M. G., Smith, S. J., Thompson, A., van Aardenne, J., van der Werf, G. R., and van Vuuren, D. P.: Evolution of anthropogenic and biomass burning emissions of air pollutants at global and regional scales during the 1980-2010 period, Climatic Change, 109, 163–190, doi:10.1007/S10584-011-0154-1, 2011.

Grell, G. A. and Devenyi, D.: A generalized approach to parameterizing convection combining ensemble and data assimilation techniques, Geophys. Res. Lett., 29, 1693, doi:10.1029/2002gl015311, 2002.

Grell, G. A., Peckham, S. E., Schmitz, R., McKeen, S. A., Frost, G., Skamarock, W. C., and Eder, B.: Fully coupled "online" chemistry within the WRF model, Atmos. Environ., 39, 6957–6975, doi:10.1016/J.Atmosenv.2005.04.027, 2005.

Gustafson Jr., W. I., Qian, Y., and Fast, J. D.: Downscaling aerosols and the impact of neglected subgrid processes on direct aerosol radiative forcing for a representative global climate model grid spacing, J. Geophys. Res.-Atmos., 116, D13303, doi:10.1029/2010jd015480, 2011.

Gustafson Jr., W. I., Ma, P.-L., Xiao, H., Singh, B., Rasch, P. J., and Fast, J. D.: The Separate Physics and Dynamics Experiment (SPADE) Framework for Determining Resolution Awareness: A Case Study of Microphysics, J. Geophys. Res.-Atmos., 118, 9258–9276, doi:10.1002/jgrd.50711, 2013.

Haywood, J., Bush, M., Abel, S., Claxton, B., Coe, H., Crosier, J., Harrison, M., Macpherson, B., Naylor, M., and Osborne, S.: Prediction of visibility and aerosol within the operational Met Office Unified Model. II: Validation of model performance using observational data, Q. J. Roy. Meteorol. Soc., 134, 1817–1832, doi:10.1002/Qj.275, 2008.

Holben, B. N., Eck, T. F., Slutsker, I., Tanre, D., Buis, J. P., Setzer, A., Vermote, E., Reagan, J. A., Kaufman, Y. J., Nakajima, T., Lavenu, F., Jankowiak, I., and Smirnov, A.: AERONET – A federated instrument network and data archive for aerosol characterization, Remote Sens. Environ., 66, 1–16, doi:10.1016/S0034-4257(98)00031-5, 1998.

Hong, S. Y., Juang, H. M. H., and Zhao, Q. Y.: Implementation of prognostic cloud scheme for a regional spectral model, Mon. Weather Rev., 126, 2621–2639, doi:10.1175/1520-0493(1998)126<2621:Iopcsf>2.0.Co;2, 1998.

Hurrell, J. W., Holland, M. M., Gent, P. R., Ghan, S., Kay, J. E., Kushner, P. J., Lamarque, J.-F., Large, W. G., Lawrence, D., Lindsay, K., Lipscomb, W. H., Long, M. C., Mahowald, N., Marsh, D. R., Neale, R. B., Rasch, P., Vavrus, S., Vertenstein,

M., Bader, D., Collins, W. D., Hack, J. J., Kiehl, J., and Marshall, S.: The community Earth system model: A framework for collaborative research, B. Am. Meteorol. Soc., 94, 1319–1360, doi:10.1175/BAMS-D-12-00121, 2013.

Iacono, M. J., Delamere, J. S., Mlawer, E. J., Shephard, M. W., Clough, S. A., and Collins, W. D.: Radiative forcing by long-lived greenhouse gases: Calculations with the AER radiative transfer models, J. Geophys. Res.-Atmos., 113, D13103, doi:10.1029/2008jd009944, 2008.

Iorio, J. P., Duffy, P. B., Govindasamy, B., Thompson, S. L., Khairoutdinov, M., and Randall, D.: Effects of model resolution and subgrid-scale physics on the simulation of precipitation in the continental United States, Clim. Dynam., 23, 243–258, doi:10.1007/S00382-004-0440-Y, 2004.

Jackson, R. C., McFarquhar, G. M., Korolev, A. V., Earle, M. E., Liu, P. S. K., Lawson, R. P., Brooks, S., Wolde, M., Laskin, A., and Freer, M.: The dependence of ice microphysics on aerosol concentration in arctic mixed-phase stratus clouds during IS-DAC and M-PACE, J. Geophys. Res.-Atmos., 117, D15207, doi:10.1029/2012jd017668, 2012.

Jacob, D. J., Prather, M. J., Rasch, P. J., Shia, R. L., Balkanski, Y. J., Beagley, S. R., Bergmann, D. J., Blackshear, W. T., Brown, M., Chiba, M., Chipperfield, M. P., deGrandpre, J., Dignon, J. E., Feichter, J., Genthon, C., Grose, W. L., Kasibhatla, P. S., Kohler, I., Kritz, M. A., Law, K., Penner, J. E., Ramonet, M., Reeves, C. E., Rotman, D. A., Stockwell, D. Z., VanVelthoven, P. F. J., Verver, G., Wild, O., Yang, H., and Zimmermann, P.: Evaluation and intercomparison of global atmospheric transport models using Rn-222 and other short-lived tracers, J. Geophys. Res.-Atmos., 102, 5953–5970, doi:10.1029/96jd02955, 1997.

Jacob, D. J., Crawford, J. H., Maring, H., Clarke, A. D., Dibb, J. E., Emmons, L. K., Ferrare, R. A., Hostetler, C. A., Russell, P. B., Singh, H. B., Thompson, A. M., Shaw, G. E., McCauley, E., Pederson, J. R., and Fisher, J. A.: The Arctic Research of the Composition of the Troposphere from Aircraft and Satellites (ARCTAS) mission: design, execution, and first results, Atmos. Chem. Phys., 10, 5191–5212, doi:10.5194/acp-10-5191-2010, 2010.

Janjic, Z. I.: Nonsingular Implementation of the Mellor–Yamada Level 2.5 Scheme in the NCEP Meso model, NCEP Office Note, No. 437, 61 pp., 2002.

Kanamaru, H. and Kanamitsu, M.: Scale-selective bias correction in a downscaling of global analysis using a regional model, Mon. Weather Rev., 135, 334–350, doi:10.1175/Mwr3294.1, 2007.

Kang, I. S., Jin, K., Wang, B., Lau, K. M., Shukla, J., Krishnamurthy, V., Schubert, S. D., Wailser, D. E., Stern, W. F., Kitoh, A., Meehl, G. A., Kanamitsu, M., Galin, V. Y., Satyan, V., Park, C. K., and Liu, Y.: Intercomparison of the climatological variations of Asian summer monsoon precipitation simulated by 10 GCMs, Clim. Dynam., 19, 383–395, doi:10.1007/S00382-002-0245-9, 2002.

Koch, D., Schulz, M., Kinne, S., McNaughton, C., Spackman, J. R., Balkanski, Y., Bauer, S., Berntsen, T., Bond, T. C., Boucher, O., Chin, M., Clarke, A., De Luca, N., Dentener, F., Diehl, T., Dubovik, O., Easter, R., Fahey, D. W., Feichter, J., Fillmore, D., Freitag, S., Ghan, S., Ginoux, P., Gong, S., Horowitz, L., Iversen, T., Kirkevåg, A., Klimont, Z., Kondo, Y., Krol, M., Liu, X., Miller, R., Montanaro, V., Moteki, N., Myhre, G., Penner, J. E., Perlwitz, J., Pitari, G., Reddy, S., Sahu, L., Sakamoto, H., Schuster, G., Schwarz, J. P., Seland, Ø., Stier, P., Takegawa, N.,

Takemura, T., Textor, C., van Aardenne, J. A., and Zhao, Y.: Evaluation of black carbon estimations in global aerosol models, Atmos. Chem. Phys., 9, 9001–9026, doi:10.5194/acp-9-9001-2009, 2009.

Kooperman, G. J., Pritchard, M. S., Ghan, S. J., Wang, M. H., Somerville, R. C. J., and Russell, L. M.: Constraining the influence of natural variability to improve estimates of global aerosol indirect effects in a nudged version of the Community Atmosphere Model 5, J. Geophys. Res.-Atmos., 117, D23204, doi:10.1029/2012jd018588, 2012.

Kravitz, B., Robock, A., Boucher, O., Schmidt, H., Taylor, K. E., Stenchikov, G., and Schulz, M.: The Geoengineering Model Intercomparison Project (GeoMIP), Atmos. Sci. Lett., 12, 162–167, doi:10.1002/Asl.316, 2011.

Lamarque, J.-F., Emmons, L. K., Hess, P. G., Kinnison, D. E., Tilmes, S., Vitt, F., Heald, C. L., Holland, E. A., Lauritzen, P. H., Neu, J., Orlando, J. J., Rasch, P. J., and Tyndall, G. K.: CAM-chem: description and evaluation of interactive atmospheric chemistry in the Community Earth System Model, Geosci. Model Dev., 5, 369–411, doi:10.5194/gmd-5-369-2012, 2012.

Laprise, R., de Elia, R., Caya, D., Biner, S., Lucas-Picher, P., Diaconescu, E., Leduc, M., Alexandru, A., Separovic, L., and Climate, C. N. R.: Challenging some tenets of Regional Climate Modelling, Meteorol. Atmos. Phys., 100, 3–22, doi:10.1007/S00703-008-0292-9, 2008.

Law, K. S. and Stohl, A.: Arctic air pollution: Origins and impacts, Science, 315, 1537–1540, doi:10.1126/Science.1137695, 2007.

Lawrence, M. G., Crutzen, P. J., Rasch, P. J., Eaton, B. E., and Mahowald, N. M.: A model for studies of tropospheric photochemistry: Description, global distributions, and evaluation, J. Geophys. Res.-Atmos., 104, 26245–26277, doi:10.1029/1999jd900425, 1999.

Lee, Y. H., Lamarque, J.-F., Flanner, M. G., Jiao, C., Shindell, D. T., Berntsen, T., Bisiaux, M. M., Cao, J., Collins, W. J., Curran, M., Edwards, R., Faluvegi, G., Ghan, S., Horowitz, L. W., McConnell, J. R., Ming, J., Myhre, G., Nagashima, T., Naik, V., Rumbold, S. T., Skeie, R. B., Sudo, K., Takemura, T., Thevenon, F., Xu, B., and Yoon, J.-H.: Evaluation of preindustrial to present-day black carbon and its albedo forcing from Atmospheric Chemistry and Climate Model Intercomparison Project (ACCMIP), Atmos. Chem. Phys., 13, 2607–2634, doi:10.5194/acp-13-2607-2013, 2013.

Leung, L. R.: Regional Climate Models, In Encyclopedia of Sustainability Science and Technology, edited by: Meyers, R. A., 7365–7381, Springer, New York, 2012.

Leung, L. R. and Ghan, S. J.: Pacific Northwest climate sensitivity simulated by a regional climate model driven by a GCM. Part I: Control simulations, J. Climate, 12, 2010–2030, doi:10.1175/1520-0442(1999)012<2010:Pncssb>2.0.Co;2, 1999a.

Leung, L. R. and Ghan, S. J.: Pacific northwest climate sensitivity simulated by a regional climate model driven by a GCM. Part II: 2xCO(2) simulations, J. Climate, 12, 2031–2053, doi:10.1175/1520-0442(1999)012<2031:Pncssb>2.0.Co;2, 1999b.

Leung, L. R. and Qian, Y.: The sensitivity of precipitation and snowpack simulations to model resolution via nesting in regions of complex terrain, J. Hydrometeorol., 4, 1025–1043,

doi:10.1175/1525-7541(2003)004<1025:Tsopas>2.0.Co;2, 2003.

Leung, L. R., Qian, Y., and Bian, X. D.: Hydroclimate of the western United States based on observations and regional climate simulation of 1981–2000. part I: Seasonal statistics, J. Climate, 16, 1892–1911, doi:10.1175/1520-0442(2003)016<1892:Hotwus>2.0.Co;2, 2003a.

Leung, L. R., Qian, Y., Bian, X. D., and Hunt, A.: Hydroclimate of the western United States based on observations and regional climate simulation of 1981–2000. part II: Mesoscale ENSO anomalies, J. Climate, 16, 1912–1928, doi:10.1175/1520-0442(2003)016<1912:Hotwus>2.0.Co;2, 2003b.

Leung, L. R., Qian, Y., Bian, X. D., Washington, W. M., Han, J. G., and Roads, J. O.: Mid-century ensemble regional climate change scenarios for the western United States, Climatic Change, 62, 75–113, doi:10.1023/B:Clim.0000013692.50640.55, 2004.

Leung, L. R., Kuo, Y. H., and Tribbia, J.: Research needs and directions of regional climate modeling using WRF and CCSM, B. Am. Meteorol. Soc., 87, 1747–1751, doi:10.1175/Bams-887-12-1747, 2006.

Li, F. Y., Collins, W. D., Wehner, M. F., Williamson, D. L., Olson, J. G., and Algieri, C.: Impact of horizontal resolution on simulation of precipitation extremes in an aqua-planet version of Community Atmospheric Model (CAM3), Tellus A, 63, 884–892, doi:10.1111/J.1600-0870.2011.00544.X, 2011.

Liang, J., Wu, L. G., Ge, X. Y., and Wu, C. C.: Monsoonal Influence on Typhoon Morakot (2009). Part II: Numerical Study, J. Atmos. Sci., 68, 2222–2235, doi:10.1175/2011jas3731.1, 2011.

Liang, X. Z., Kunkel, K. E., and Samel, A. N.: Development of a regional climate model for US midwest applications. Part I: Sensitivity to buffer zone treatment, J. Climate, 14, 4363–4378, doi:10.1175/1520-0442(2001)014<4363:Doarcm>2.0.Co;2, 2001.

Liang, X. Z., Pan, J. P., Zhu, J. H., Kunkel, K. E., Wang, J. X. L., and Dai, A.: Regional climate model downscaling of the U.S. summer climate and future change, J. Geophys. Res.-Atmos., 111, D10108, doi:10.1029/2005jd006685, 2006.

Liao, L. and Sassen, K.: Investigation of Relationships between Ka-Band Radar Reflectivity and Ice and Liquid Water Contents, Atmos. Res., 34, 231–248, 1994.

Lin, I. I., Chou, M. D., and Wu, C. C.: The Impact of a Warm Ocean Eddy on Typhoon Morakot (2009): A Preliminary Study from Satellite Observations and Numerical Modelling, Terr. Atmos. Ocean. Sci., 22, 661–671, doi:10.3319/Tao.2011.08.19.01(Tm), 2011.

Liu, C. L. and Illingworth, A. J.: Toward more accurate retrievals of ice water content from radar measurements of clouds, J. Appl. Meteorol., 39, 1130–1146, doi:10.1175/1520-0450(2000)039<1130:Tmaroi>2.0.Co;2, 2000.

Liu, J. F., Mauzerall, D. L., Horowitz, L. W., Ginoux, P., and Fiore, A. M.: Evaluating inter-continental transport of fine aerosols: (1) Methodology, global aerosol distribution and optical depth, Atmos. Environ., 43, 4327–4338, doi:10.1016/J.Atmosenv.2009.03.054, 2009.

Liu, X., Easter, R. C., Ghan, S. J., Zaveri, R., Rasch, P., Shi, X., Lamarque, J.-F., Gettelman, A., Morrison, H., Vitt, F., Conley, A., Park, S., Neale, R., Hannay, C., Ekman, A. M. L., Hess, P., Mahowald, N., Collins, W., Iacono, M. J., Bretherton, C. S., Flanner, M. G., and Mitchell, D.: Toward a minimal representation

of aerosols in climate models: description and evaluation in the Community Atmosphere Model CAM5, Geosci. Model Dev., 5, 709–739, doi:10.5194/gmd-5-709-2012, 2012.

Liu, X., Ma, P.-L., Zhao, C., Gattiker, J. R., and Rasch, P. J.: Quantifying the uncertainty of aerosol indirect forcing in CAM5, Environ. Res. Lett., in preparation, 2014.

Ma, P.-L., Zhang, K., Shi, J. J., Matsui, T., and Arking, A.: Direct Radiative Effect of Mineral Dust on the Development of African Easterly Waves in Late Summer, 2003–07, J. Appl. Meteorol. Clim., 51, 2090–2104, doi:10.1175/Jamc-D-11-0215.1, 2012.

Ma, P.-L., Gattiker, J. R., Liu, X. H., and Rasch, P. J.: A novel approach for determining source-receptor relationships in model simulations: a case study of black carbon transport in northern hemisphere winter, Environ. Res. Lett., 8, 024042, doi:10.1088/1748-9326/8/2/024042, 2013a.

Ma, P.-L., Rasch, P. J., Wang, H., Zhang, K., Easter, R. C., Tilmes, S., Fast, J. D., Liu, X., Yoon, J.-H., and Lamarque, J.-F.: The role of circulation features on black carbon transport into the Arctic in the Community Atmosphere Model version 5 (CAM5), J. Geophys. Res. Atmos., 118, 4657–4669, doi:10.1002/jgrd.50411, 2013b.

Marshall, S., Roads, J. O., and Oglesby, R. J.: Effects of resolution and physics on precipitation in the NCAR Community Climate Model, J. Geophys. Res.-Atmos., 102, 19529–19541, doi:10.1029/97jd01428, 1997.

McComiskey, A. and Feingold, G.: The scale problem in quantifying aerosol indirect effects, Atmos. Chem. Phys., 12, 1031–1049, doi:10.5194/acp-12-1031-2012, 2012.

McFarquhar, G. M., Ghan, S., Verlinde, J., Korolev, A., Strapp, J. W., Schmid, B., Tomlinson, J. M., Wolde, M., Brooks, S. D., Cziczo, D., Dubey, M. K., Fan, J. W., Flynn, C., Gultepe, I., Hubbe, J., Gilles, M. K., Laskin, A., Lawson, P., Leaitch, W. R., Liu, P., Liu, X. H., Lubin, D., Mazzoleni, C., Macdonald, A. M., Moffet, R. C., Morrison, H., Ovchinnikov, M., Shupe, M. D., Turner, D. D., Xie, S. C., Zelenyuk, A., Bae, K., Freer, M., and Glen, A.: Indirect and Semi-Direct Aerosol Campaign the Impact of Arctic Aerosols on Clouds, B. Am. Meteorol. Soc., 92, 183–201, doi:10.1175/2010bams2935.1, 2011.

McNaughton, C. S., Clarke, A. D., Freitag, S., Kapustin, V. N., Kondo, Y., Moteki, N., Sahu, L., Takegawa, N., Schwarz, J. P., Spackman, J. R., Watts, L., Diskin, G., Podolske, J., Holloway, J. S., Wisthaler, A., Mikoviny, T., de Gouw, J., Warneke, C., Jimenez, J., Cubison, M., Howell, S. G., Middlebrook, A., Bahreini, R., Anderson, B. E., Winstead, E., Thornhill, K. L., Lack, D., Cozic, J., and Brock, C. A.: Absorbing aerosol in the troposphere of the Western Arctic during the 2008 ARC-TAS/ARCPAC airborne field campaigns, Atmos. Chem. Phys., 11, 7561–7582, doi:10.5194/acp-11-7561-2011, 2011.

Meehl, G. A., Covey, C., McAvaney, B., Latif, M., and Stouffer, R. J.: Overview of the Coupled Model Intercomparison Project, B. Am. Meteorol. Soc., 86, 89–93, doi:10.1175/Bams-86-1-89, 2005.

Meehl, G. A., Washington, W. M., Arblaster, J. M., Hu, A. X., Teng, H. Y., Tebaldi, C., Sanderson, B. N., Lamarque, J. F., Conley, A., Strand, W. G., and White, J. B.: Climate System Response to External Forcings and Climate Change Projections in CCSM4, J. Climate, 25, 3661–3683, doi:10.1175/Jcli-D-11-00240.1, 2012.

Mellor, G. L. and Yamada, T.: Development of a Turbulence Closure-Model for Geophysical Fluid Problems, Rev. Geophys., 20, 851–875, doi:10.1029/Rg020i004p00851, 1982.

Mlawer, E. J., Taubman, S. J., Brown, P. D., Iacono, M. J., and Clough, S. A.: Radiative transfer for inhomogeneous atmospheres: RRTM, a validated correlated-k model for the longwave, J. Geophys. Res.-Atmos., 102, 16663–16682, doi:10.1029/97jd00237, 1997.

Morrison, H. and Gettelman, A.: A new two-moment bulk stratiform cloud microphysics scheme in the community atmosphere model, version 3 (CAM3). Part I: Description and numerical tests, J. Climate, 21, 3642–3659, doi:10.1175/2008jcli2105.1, 2008.

Morrison, H., Thompson, G., and Tatarskii, V.: Impact of Cloud Microphysics on the Development of Trailing Stratiform Precipitation in a Simulated Squall Line: Comparison of One- and Two-Moment Schemes, Mon. Weather Rev., 137, 991–1007, doi:10.1175/2008mwr2556.1, 2009.

Neale, R. B., Richter, J. H., and Jochum, M.: The Impact of Convection on ENSO: From a Delayed Oscillator to a Series of Events, J. Climate, 21, 5904–5924, doi:10.1175/2008jcli2244.1, 2008.

Neale, R. B., Chen, C.-C., Gettelman, A., Lauritzen, P. H., Park, S., Williamson, D. L., Conley, A. J., Garcia, R., Kinnison, D., Lamarque, J.-F., Marsh, D., Mills, M., Smith, A. K., Tilmes, S., Vitt, F., Cameron-Smith, P., Collins, W. D., Iacono, M. J., Easter, R. C., Ghan, S. J., Liu, X., Rasch, P. J., and Taylor, M. A.: Description of the NCAR Community Atmosphere Model (CAM5), Technical Report NCAR/TN-486+STR, National Center for Atmospheric Research, Boulder, Colorado, 268 pp., 2010.

Ovtchinnikov, M. and Ghan, S. J.: Parallel simulations of aerosol influence on clouds using cloud-resolving and single-column models, J. Geophys. Res.-Atmos., 110, D15S10, doi:10.1029/2004jd005088, 2005.

Park, S. and Bretherton, C. S.: The University of Washington Shallow Convection and Moist Turbulence Schemes and Their Impact on Climate Simulations with the Community Atmosphere Model, J. Climate, 22, 3449–3469, doi:10.1175/2008jcli2557.1, 2009.

Park, S., Bretherton, C. S., and Rasch, P. J.: Global Cloud Simulation in the Community Atmosphere Model 5, J. Climate, submitted, 2014.

Posselt, R. and Lohmann, U.: Sensitivity of the total anthropogenic aerosol effect to the treatment of rain in a global climate model, Geophys. Res. Lett., 36, L02805, doi:10.1029/2008gl035796, 2009.

Qian, Y., Gustafson Jr., W. I., and Fast, J. D.: An investigation of the sub-grid variability of trace gases and aerosols for global climate modeling, Atmos. Chem. Phys., 10, 6917–6946, doi:10.5194/acp-10-6917-2010, 2010.

Quaas, J., Ming, Y., Menon, S., Takemura, T., Wang, M., Penner, J. E., Gettelman, A., Lohmann, U., Bellouin, N., Boucher, O., Sayer, A. M., Thomas, G. E., McComiskey, A., Feingold, G., Hoose, C., Kristjánsson, J. E., Liu, X., Balkanski, Y., Donner, L. J., Ginoux, P. A., Stier, P., Grandey, B., Feichter, J., Sednev, I., Bauer, S. E., Koch, D., Grainger, R. G., Kirkevåg, A., Iversen, T., Seland, Ø., Easter, R., Ghan, S. J., Rasch, P. J., Morrison, H., Lamarque, J.-F., Iacono, M. J., Kinne, S., and Schulz, M.: Aerosol indirect effects – general circulation model compar-

parison and evaluation with satellite data, Atmos. Chem. Phys., 9, 8697–8717, doi:10.5194/acp-9-8697-2009, 2009.

Quinn, P. K., Shaw, G., Andrews, E., Dutton, E. G., Ruoho-Airola, T., and Gong, S. L.: Arctic haze: current trends and knowledge gaps, Tellus B, 59, 99–114, doi:10.1111/J.1600-0889.2006.00238.X, 2007.

Ramanathan, V. and Carmichael, G.: Global and regional climate changes due to black carbon, Nat. Geosci., 1, 221–227, doi:10.1038/Ngeo156, 2008.

Rasch, P. J. and Kristjansson, J. E.: A comparison of the CCM3 model climate using diagnosed and predicted condensate parameterizations, J. Climate, 11, 1587–1614, doi:10.1175/1520-0442(1998)011<1587:Acotcm>2.0.Co;2, 1998.

Rasch, P. J., Mahowald, N. M., and Eaton, B. E.: Representations of transport, convection, and the hydrologic cycle in chemical transport models: Implications for the modeling of short-lived and soluble species, J. Geophys. Res.-Atmos., 102, 28127–28138, doi:10.1029/97jd02087, 1997.

Rasch, P. J., Feichter, J., Law, K., Mahowald, N., Penner, J., Benkovitz, C., Genthon, C., Giannakopoulos, C., Kasibhatla, P., Koch, D., Levy, H., Maki, T., Prather, M., Roberts, D. L., Roelofs, G. J., Stevenson, D., Stockwell, Z., Taguchi, S., Kritz, M., Chipperfield, M., Baldocchi, D., McMurry, P., Barrie, L., Balkansi, Y., Chatfield, R., Kjellstrom, E., Lawrence, M., Lee, H. N., Lelieveld, J., Noone, K. J., Seinfeld, J., Stenchikov, G., Schwartz, S., Walcek, C., and Williamson, D.: A comparison of scavenging and deposition processes in global models: results from the WCRP Cambridge Workshop of 1995, Tellus B, 52, 1025–1056, doi:10.1034/J.1600-0889.2000.00980.X, 2000.

Richter, J. H. and Rasch, P. J.: Effects of convective momentum transport on the atmospheric circulation in the community atmosphere model, version 3, J. Climate, 21, 1487–1499, doi:10.1175/2007jcli1789.1, 2008.

Rind, D., Lerner, J., Jonas, J., and McLinden, C.: Effects of resolution and model physics on tracer transports in the NASA Goddard Institute for Space Studies general circulation models, J. Geophys. Res.-Atmos., 112, D09315, doi:10.1029/2006jd007476, 2007.

Roeckner, E., Brokopf, R., Esch, M., Giorgetta, M., Hagemann, S., Kornblueh, L., Manzini, E., Schlese, U., and Schulzweida, U.: Sensitivity of simulated climate to horizontal and vertical resolution in the ECHAM5 atmosphere model, J. Climate, 19, 3771–3791, doi:10.1175/Jcli3824.1, 2006.

Screen, J. A. and Simmonds, I.: The central role of diminishing sea ice in recent Arctic temperature amplification, Nature, 464, 1334–1337, doi:10.1038/Nature09051, 2010.

Serreze, M. C., Barrett, A. P., Stroeve, J. C., Kindig, D. N., and Holland, M. M.: The emergence of surface-based Arctic amplification, The Cryosphere, 3, 11–19, doi:10.5194/tc-3-11-2009, 2009.

Sharma, S., Andrews, E., Barrie, L. A., Ogren, J. A., and Lavoue, D.: Variations and sources of the equivalent black carbon in the high Arctic revealed by long-term observations at Alert and Barrow: 1989–2003, J. Geophys. Res.-Atmos., 111, D14208, doi:10.1029/2005jd006581, 2006.

Shindell, D. T., Chin, M., Dentener, F., Doherty, R. M., Faluvegi, G., Fiore, A. M., Hess, P., Koch, D. M., MacKenzie, I. A., Sanderson, M. G., Schultz, M. G., Schulz, M., Stevenson, D. S., Teich, H., Textor, C., Wild, O., Bergmann, D. J., Bey, I., Bian, H., Cuvelier, C., Duncan, B. N., Folberth, G., Horowitz, L. W., Jonson, J.,

Kaminski, J. W., Marmer, E., Park, R., Pringle, K. J., Schroeder, S., Szopa, S., Takemura, T., Zeng, G., Keating, T. J., and Zuber, A.: A multi-model assessment of pollution transport to the Arctic, Atmos. Chem. Phys., 8, 5353–5372, doi:10.5194/acp-8-5353-2008, 2008.

Skamarock, W. C., Klemp, J. B., Dudhia, J., Gill, D. O., Barker, D. M., Duda, M. G., Wang, W., and Powers, J. G.: A description of the advanced research WRF version 3, NCAR Technical Note, NCAR/TN-475+STR, National Center for Atmospheric Research, Boulder, Colorado, 113 pp., 2008.

Skamarock, W. C., Klemp, J. B., Duda, M. G., Fowler, L. D., Park, S. H., and Ringler, T. D.: A Multiscale Nonhydrostatic Atmospheric Model Using Centroidal Voronoi Tesselations and C-Grid Staggering, Mon. Weather Rev., 140, 3090–3105, doi:10.1175/Mwr-D-11-00215.1, 2012.

Spackman, J. R., Gao, R. S., Neff, W. D., Schwarz, J. P., Watts, L. A., Fahey, D. W., Holloway, J. S., Ryerson, T. B., Peischl, J., and Brock, C. A.: Aircraft observations of enhancement and depletion of black carbon mass in the springtime Arctic, Atmos. Chem. Phys., 10, 9667–9680, doi:10.5194/acp-10-9667-2010, 2010.

Stohl, A., Klimont, Z., Eckhardt, S., Kupiainen, K., Shevchenko, V. P., Kopeikin, V. M., and Novigatsky, A. N.: Black carbon in the Arctic: the underestimated role of gas flaring and residential combustion emissions, Atmos. Chem. Phys., 13, 8833–8855, doi:10.5194/acp-13-8833-2013, 2013.

Taylor, K. E., Stouffer, R. J., and Meehl, G. A.: An Overview of Cmip5 and the Experiment Design, B. Am. Meteorol. Soc., 93, 485–498, doi:10.1175/Bams-D-11-00094.1, 2012.

Teng, H. Y., Washington, W. M., Branstator, G., Meehl, G. A., and Lamarque, J. F.: Potential impacts of Asian carbon aerosols on future US warming, Geophys. Res. Lett., 39, L11703, doi:10.1029/2012gl051723, 2012.

Textor, C., Schulz, M., Guibert, S., Kinne, S., Balkanski, Y., Bauer, S., Berntsen, T., Berglen, T., Boucher, O., Chin, M., Dentener, F., Diehl, T., Easter, R., Feichter, H., Fillmore, D., Ghan, S., Ginoux, P., Gong, S., Grini, A., Hendricks, J., Horowitz, L., Huang, P., Isaksen, I., Iversen, I., Kloster, S., Koch, D., Kirkevåg, A., Kristjansson, J. E., Krol, M., Lauer, A., Lamarque, J. F., Liu, X., Montanaro, V., Myhre, G., Penner, J., Pitari, G., Reddy, S., Seland, Ø., Stier, P., Takemura, T., and Tie, X.: Analysis and quantification of the diversities of aerosol life cycles within AeroCom, Atmos. Chem. Phys., 6, 1777–1813, doi:10.5194/acp-6-1777-2006, 2006.

von Storch, H., Langenberg, H., and Feser, F.: A spectral nudging technique for dynamical downscaling purposes, Mon. Weather Rev., 128, 3664–3673, doi:10.1175/1520-0493(2000)128<3664:Asntfd>2.0.Co;2, 2000.

Wang, H. and Feingold, G.: Modeling Mesoscale Cellular Structures and Drizzle in Marine Stratocumulus. Part II: The Microphysics and Dynamics of the Boundary Region between Open and Closed Cells, J. Atmos. Sci., 66, 3257–3275, doi:10.1175/2009jas3120.1, 2009a.

Wang, H. and Feingold, G.: Modeling Mesoscale Cellular Structures and Drizzle in Marine Stratocumulus. Part I: Impact of Drizzle on the Formation and Evolution of Open Cells, J. Atmos Sci, 66, 3237–3256, doi:10.1175/2009jas3022.1, 2009b.

Wang, H., Easter, R. C., Rasch, P. J., Wang, M., Liu, X., Ghan, S. J., Qian, Y., Yoon, J.-H., Ma, P.-L., and Vinoj, V.: Sensitivity of remote aerosol distributions to representation of cloud-aerosol

interactions in a global climate model, Geosci. Model Dev., 6, 765–782, doi:10.5194/gmd-6-765-2013, 2013.

Wang, M., Ghan, S., Ovchinnikov, M., Liu, X., Easter, R., Kassianov, E., Qian, Y., and Morrison, H.: Aerosol indirect effects in a multi-scale aerosol-climate model PNNL-MMF, Atmos. Chem. Phys., 11, 5431–5455, doi:10.5194/acp-11-5431-2011, 2011.

Wang, M., Ghan, S., Liu, X., L'Ecuyer, T. S., Zhang, K., Morrison, H., Ovchinnikov, M., Easter, R., Marchand, R., Chand, D., Qian, Y., and Penner, J. E.: Constraining cloud lifetime effects of aerosols using A-Train satellite observations, Geophys. Res. Lett., 39, L15709, doi:10.1029/2012gl052204, 2012.

Wang, Q., Jacob, D. J., Fisher, J. A., Mao, J., Leibensperger, E. M., Carouge, C. C., Le Sager, P., Kondo, Y., Jimenez, J. L., Cubison, M. J., and Doherty, S. J.: Sources of carbonaceous aerosols and deposited black carbon in the Arctic in winter-spring: implications for radiative forcing, Atmos. Chem. Phys., 11, 12453–12473, doi:10.5194/acp-11-12453-2011, 2011.

Wang, Y. X. X., McElroy, M. B., Jacob, D. J., and Yantosca, R. M.: A nested grid formulation for chemical transport over Asia: Applications to CO, J. Geophys. Res.-Atmos., 109, D22307, doi:10.1029/2004jd005237, 2004.

Weigum, N. M., Stier, P., Schwarz, J. P., Fahey, D. W., and Spackman, J. R.: Scales of variability of black carbon plumes over the Pacific Ocean, Geophys. Res. Lett., 39, L15804, doi:10.1029/2012gl052127, 2012.

Wiedinmyer, C., Akagi, S. K., Yokelson, R. J., Emmons, L. K., Al-Saadi, J. A., Orlando, J. J., and Soja, A. J.: The Fire INventory from NCAR (FINN): a high resolution global model to estimate the emissions from open burning, Geosci. Model Dev., 4, 625–641, doi:10.5194/gmd-4-625-2011, 2011.

Williamson, D. L.: Time-split versus process-split coupling of parameterizations and dynamical core, Mon. Weather Rev., 130, 2024–2041, doi:10.1175/1520-0493(2002)130<2024:Tsvpsc>2.0.Co;2, 2002.

Williamson, D. L.: The effect of time steps and time-scales on parametrization suites, Q. J. Roy. Meteorol. Soc., 139, 548–560, doi:10.1002/Qj.1992, 2013.

Wu, W. L., Lynch, A. H., and Rivers, A.: Estimating the uncertainty in a regional climate model related to initial and lateral boundary conditions, J. Climate, 18, 917–933, doi:10.1175/Jcli-3293.1, 2005.

Xie, S. C., McCoy, R. B., Klein, S. A., Cederwall, R. T., Wiscombe, W. J., Clothiaux, E. E., Gaustad, K. L., Golaz, J. C., Hall, S. D., Jensen, M. P., Johnson, K. L., Lin, Y. L., Long, C. N., Mather, J. H., McCord, R. A., McFarlane, S. A., Palanisamy, G., Shi, Y., and Turner, D. D. D.: Arm Climate Modeling Best Estimate Data a New Data Product for Climate Studies, B. Am. Meteorol. Soc., 91, 13–20, doi:10.1175/2009bams2891.1, 2010.

Yang, Q., Gustafson Jr., W. I., Fast, J. D., Wang, H., Easter, R. C., Wang, M., Ghan, S. J., Berg, L. K., Leung, L. R., and Morrison, H.: Impact of natural and anthropogenic aerosols on stratocumulus and precipitation in the Southeast Pacific: a regional modelling study using WRF-Chem, Atmos. Chem. Phys., 12, 8777–8796, doi:10.5194/acp-12-8777-2012, 2012.

Zaveri, R. A. and Peters, L. K.: A new lumped structure photochemical mechanism for large-scale applications, J. Geophys. Res.-Atmos., 104, 30387–30415, doi:10.1029/1999jd900876, 1999.

Zaveri, R. A., Easter, R. C., Fast, J. D., and Peters, L. K.: Model for Simulating Aerosol Interactions and Chem-

istry (MOSAIC), J. Geophys. Res.-Atmos., 113, D13204, doi:10.1029/2007jd008782, 2008.

Zhang, G. J. and Mcfarlane, N. A.: Sensitivity of Climate Simulations to the Parameterization of Cumulus Convection in the Canadian Climate Center General-Circulation Model, Atmos. Ocean., 33, 407–446, 1995.

Zhang, H., Fraedrich, K., Blender, R., and Zhu, X. H.: Precipitation Extremes in CMIP5 Simulations on Different Time Scales, J. Hydrometeorol., 14, 923–928, doi:10.1175/Jhm-D-12-0181.1, 2013.

Zhang, L. M., Gong, S. L., Padro, J., and Barrie, L.: A size-segregated particle dry deposition scheme for an atmospheric aerosol module, Atmos. Environ., 35, 549–560, doi:10.1016/S1352-2310(00)00326-5, 2001.

Zhao, C. F., Xie, S. C., Klein, S. A., Protat, A., Shupe, M. D., McFarlane, S. A., Comstock, J. M., Delanoe, J., Deng, M., Dunn, M., Hogan, R. J., Huang, D., Jensen, M. P., Mace, G. G., McCoy, R., O'Connor, E. J., Turner, D. D., and Wang, Z.: Toward understanding of differences in current cloud retrievals of ARM ground-based measurements, J. Geophys. Res.-Atmos., 117, D10206, doi:10.1029/2011jd016792, 2012.